

PARAMETRIC SENSITIVITY IN A MODEL OF A MOTOR PATTERN
GENERATOR IN *APLYSIA*

by

HSING-DUAN LOUH

Submitted in partial fulfillment of the requirements for the degree of

Master of Science

Department of Mathematics, Applied Mathematics and Statistics

CASE WESTERN RESERVE UNIVERSITY

August 2020

CASE WESTERN RESERVE UNIVERSITY
SCHOOL OF GRADUATE STUDIES

We hereby approve the thesis of

Hsing-Duan Louh

Candidate for the Degree of Master of Science *.

Prof. Peter J. Thomas

Committee Chair, Advisor

Prof. Hillel J. Chiel

External Faculty, Advisor

Prof. Wanda Strychalski

Associate Professor of Mathematics

Prof. Erkki Somersalo

Professor of Mathematics

Date: July 22, 2020

*We also certify that written approval has been obtained for any proprietary material contained therein.

Contents

Acknowledgements	iv
List of Tables	vi
List of Figures	vii
Abstract	1
1 Introduction	2
1.1 Model Equations	5
1.2 Heteroclinic and Limit Cycle Regime	12
1.3 Measuring Fitness	15
2 Sensitivity to Opening/Closing Boundary	17
2.1 Parameterizing the Open and Closed Regions	18
2.2 Model Implementation	21
3 Grasper Behaviors in Distinct Parameter Regions	27
3.1 Identifying Parameter Regions	27
3.2 Fixed Points Distinguish Parameter Regions	29
3.3 Analyzing the Parameter Regions	33
4 The Effect of Load on Fitness	41
4.1 Varying Seaweed Force across Parameter Regions	42
4.2 Collapse of the Feeding Rhythm	46
5 Discussion	55
5.1 Interpreting the Parameter Regions	55
5.2 Model Limitations	60
5.3 Future Directions	62

A Appendix	64
A.1 Parameters and Variables	64
A.2 Code	65
A.2.1 lyttle_model.m	65
A.2.2 lyttle_model_vary_grapser.m	65
A.2.3 lyttle_model_vary_grasper_run.m	65
A.2.4 lyttle_model_state_var_plots.m	68
A.2.5 Fsw_vs_IntakeRate.m	70
A.2.6 RegionGeometry.m	73
A.2.7 Rate_of_change_of_differences_dzdt.m	74
A.2.8 grasperForceCompare.m	78
References	80

Acknowledgements

This research project would not have been possible without the help and expertise from many people. I would like to thank my advisor Dr. Peter Thomas. His excitement for research coupled with his methodical approaches taught me how to transform curiosity into practical steps. I would also like to thank Dr. Hillel Chiel who has given me valuable feedback and challenged me to always think about the biological significance behind each component of a mathematical model. I am deeply grateful to both Dr. Thomas and Dr. Hillel Chiel for their guidance both in class and in research. I am thankful for Jeff Gill's mentorship. Whether I needed help on analysis, making presentations, or getting trained for slug duty, Jeff always took generous amounts of time to work with me, with humor and kindness at the ready. I would like to extend a special thank you to Dr. Yangyang Wang (University of Iowa) for sharing her implementation of the model developed by Dr. Kendrick Shaw and Dr. David Lyttle. Many thanks to Doneyear Thomas for frequently reaching out to direct me through the administrative tasks required for the master's degree and Alexander Cao for sharing his thesis template with me.

My journey as a graduate student was only possible because of my family's support. All of you have shown me endless patience and compassion, and I cannot thank you all enough.

Whether as an undergraduate or graduate student, I was surrounded by many transformative mentors and colleagues. Dr. Errki Somersalo was always willing to listen and offer me his insight, and Dr. Mark Meckes gave me invaluable encouragements during critical moments of my undergraduate years. Shusen Pu taught me how to use the High Performance Computing Cluster which saved me countless hours, and together with Alexander Strang, they introduced me to a community of passionate graduate students and helped me get my much needed weekly dose of exercise. To Anita Lu and Stephen Liu, we have shared many memorable moments and fueled each other's excitement for mathematics ever since our first course together in Analysis. Thank you Linh Huynh for your reassuring words as I wrote my

thesis. I would like to express my gratitude to all the members of the Computational Biology Lab and the Chiel lab for sharing your excitement and support during our time together.

List of Tables

1	Model State Variables	64
2	Model Parameters	64

List of Figures

1	Grasper Anatomy	7
2	Grasper Motions and Neural Pools from Shaw et al. (2015)	9
3	Neural Activation Limit Cycles from Shaw et al. (2015).	14
4	Grasper-Open and Grasper-Closed Regions in Three-Dimensions	17
5	Grasper-Open and Grasper-Closed Regions in Two Dimensions	19
6	Parameters Defining the Grasper-Closed Boundary Regions	20
7	Shaw/Lytle Model State Variables	23
8	Seaweed Ingestion Rate Estimation	24
9	The Eight Parameter Regions	27
10	Distribution of S across Parameter Regions	28
11	Switching Boundary in Different Parameter Regions	30
12	Theoretical Neural Fixed Point Regions	31
13	Parameter Regions overlaid with Fixed Point Regions	33
14	Eight Sampled Points each of the Parameter Regions	34
15	State Variables in Intake ($S > 0$) Regions I-III	35
16	State Variables in Neutral ($S = 0$) Regions	37
17	State Variables in Rejection ($S < 0$) Regions	38
18	Robustness of Different Parameter Regions against Variations in Seaweed Force	43
19	Change in Seaweed Position and Period under Different Forces	45
20	Collapse of Grasper Movement in Intake Region II	48
21	Rate of Trajectory Difference	51
22	Length-tension Curve of the I2 and I3 Muscles	52
23	Grasper Behaviors in Different Parameter Regions at $F_{sw} = 0.1162$	54
24	Adjacent Parameter Regions	59

Parametric Sensitivity in a Model of a Motor Pattern Generator in *Aplysia*

Abstract

by

HSING-DUAN LOUH

An animal's survival depends on its ability to adapt to a constantly shifting environment. Mathematical models of rhythmic motor patterns typically incorporate a central pattern generator (CPG) circuit, driving motor output in the body. In this thesis, we study Shaw and Lyttle's model for the feeding system of the marine mollusk *Aplysia californica*, which eats seaweed. The CPG has a heteroclinic channel architecture with three metastable fixed points. Using mean rate of seaweed ingestion as an objective function, we studied the system's sensitivity to parameters representing (i) the force with which seaweed opposes swallowing, and (ii) threshold and weighting parameters controlling when the feeding apparatus (grasper) opens or closes on the seaweed. We found eight motor "strategies," corresponding to whether the grasper was open or closed near each of the CPG's fixed points. In addition, we studied how rhythmic movements break down when challenged by excessively large resisting forces.

1 Introduction

An animal’s survival depends on its ability to adapt to a constantly shifting environment. For example, when we swim or dig, we do so despite different current speeds and soil density, respectively. From a dynamical systems point of view, rhythmic motions are often modeled as being driven by a *central pattern generator*, a specialized network of nerve cells that produce limit cycle dynamics. A stable limit cycle system is “robust” in the sense that if perturbed, the trajectory returns to the limit cycle, perhaps with a delay or phase shift. On the other hand, a rhythmic motor system operating under variable environmental conditions must also be “responsive”, i.e. be able to adjust its strategy or else deploy alternative strategies under different circumstances to improve performance. In order to maintain its biological fitness, a rhythmic motor system must somehow be both robust and responsive, despite changing conditions. How do organisms achieve this? One way to begin answering this question is by creating a mathematical model to incorporate details from both aspects and generate a testable hypothesis about the organism *in vivo*.

At their best, mathematical models organize disparate experimental observations into a common framework. For example, Hodgkin and Huxley consolidated many neurophysiological observations into a conductance model of the excitable membrane of the giant axon of the squid [21]. Quantitative models let biologists test hypotheses about the mechanisms underlying different behaviors. Examples include adjusting feeding rhythms to adapt to food resisting being swallowed (e.g. while eating seaweed in the marine mollusk *Aplysia californica*) [13, 22], or studying the relative contribution of feedforward versus feedback signals in controlling walking [10].

In addition, conducting “experiments” within mathematical models can suggest novel experiments to be done in the laboratory. Compared to the *in vivo* or *in vitro* laboratory experiments, mathematical models have allowed significant freedom for experimentation. Mathematical models let biologists test novel manipulations *in silico* with less expense in time and materials.

The relative ease of exploration, given a mathematical model, is a two-edged sword. In order to draw relevant conclusions, the modeller must develop a thorough understanding of the biological context, by frequent comparison of the model behavior with the biological system of of interest. Modeling may suggest parameters or interactions that lie beyond realistic ranges of values or known functional connections, so care must be taken in interpreting the results in such situations.

When creating a model, we take a minimalist approach: we attempt to include only as many details as are necessary to account for the key phenomena of interest. In modeling feeding movements in *Aplysia*, for example, we focus on robustness against the imposition of an applied load resisting ingestion of seaweed. Generally, we begin modeling with a simplified *conceptual model* [1] which we then instantiate as a *mathematical model*. As is often the case, we formulate the model by specifying a system of ordinary differential equations. In order to derive quantitative and qualitative predictions from the mathematical model, we then implement a *numerical model*, using numerical integration methods. We can subsequently affirm or discover gaps in our understanding of the biology by comparing the model results with the experimental observations [26]. Consider, for example, Hodgkin and Huxley’s model for the action potential in the squid giant axon [4]. At the conceptual level, Hodgkin and Huxley were interested in changes in current, voltage, and voltage-gated ion channels as a result of

ion movements across the membrane. These qualitative representations of the system were then used as the basis for formulating differential equations that describe a neuron's firing pattern. The Hodgkin-Huxley model were implemented and produced computational results [4] that were comparable to *in vivo* experimental data, and the relevance of their results support their conclusions about neurons.

Here, we are interested in how organisms control and adapt their rhythmic movements. Rhythmic movements are actions repeated at regular intervals such as dogs lapping water, people walking, or birds beating their wings [14]. The sea slug *Aplysia californica*'s swallowing behavior is another example of rhythmic movements. *Aplysia californica* is an ideal organism for studying motor control; it has approximately twenty thousand neurons, making its nervous system more tractable than most vertebrates [7]. A subset of these neurons reside in the buccal ganglion and stimulate the buccal mass, the feeding organ, to induce motions such as swallowing, biting, and rejection. The buccal ganglion stimulates movement by activating muscles in the feeding apparatus but also receives sensory feedback signals, which it uses to adjust ongoing rhythmic activity of the buccal mass. If a slug is interested in a particularly resistant piece of seaweed, the neurons will respond to the sensory feedback by increasing the duration and force of each bite. As with other animals, a slug's ability to adapt its rhythmic movements is critical its survival.

Dr. Kendrick Shaw and Dr. David Lyttle [13, 22] developed a phenomenological model of ingestive behavior in *Aplysia californica*. More specifically, they modeled the behavior of the sea slug's radular/odontophore (also known as the *grasper*) during biting and swallowing. The Shaw/Lyttle model can operate in two different dynamical regimes, controlled by a parameter representing endogenous excitation of the central neural circuit. The so-called *limit*

cycle regime and *heteroclinic regime*, described in the Results section of [22], are two distinct modes of rhythmic motion. A key difference between the two regimes is the sensitivity of the central circuit; in the heteroclinic regime, the circuit is more responsive to changes in sensory feedback and shows greater adaptation to changing mechanical loads. According to [22], the grasper behavior when operating in the heteroclinic regime showed greater similarity to the behavior seen *in vivo* when a load is applied to the seaweed being swallowed by the sea slug.

In this thesis, we study Shaw and Lyttle’s [13, 22] *Aplysia californica* swallowing model through parametric sensitivity analysis, in order to better understand how organisms control and adapt rhythmic movements. Beginning with the parameters of the published model, we systematically vary certain key parameters in order to investigate their qualitative and quantitative impact on the performance of the system, quantified as the average rate of food intake while swallowing an infinite uniform strip of seaweed. As we will show, variation of parameters reveals both graded changes, studied through sensitivity analysis, and discrete changes or bifurcations, leading to qualitatively different ingestion behaviors. As described above, mathematical modeling in general, and parametric analysis in particular, allows us to perform experiments that would be costly or impractical in the laboratory. Through our numerical experimentation, we hope to gain a deeper understanding of how movement is regulated in *Alpysia californica*.

1.1 Model Equations

In this thesis, we study the parametric sensitivity of the model introduced in [22]. The governing equations of the model are specified separately for activities of the neural units

(the “brain”) and the activation and displacements of motor components (the “body”):

$$\begin{aligned}\frac{d\mathbf{a}}{dt} &= \mathbf{f}(\mathbf{a}, \mu) + \epsilon \mathbf{g}(\mathbf{a}, \mathbf{x}) \\ \frac{d\mathbf{x}}{dt} &= \mathbf{h}(\mathbf{a}, \mathbf{x}) + \zeta \mathbf{l}(\mathbf{x}).\end{aligned}\tag{1}$$

The vector $\mathbf{a} = (a_0, a_1, a_2)$ is the state variable representing the the neural activities of the three pools of *Aplysia californica*’s motor neurons. The function $\mathbf{f}(\mathbf{a}, \mathbf{x})$ describes the neural dynamics, that is, how the neurons interacts with one another. The sensory feedback function $\mathbf{g}(\mathbf{a}, \mathbf{x})$ influences the neural dynamics, using information reflecting the response by the periphery, or the body. The rate of change of \mathbf{x} , the grasper position, is governed by the muscle dynamics function $\mathbf{h}(\mathbf{a}, \mathbf{x})$ and the external load $\mathbf{l}(\mathbf{x})$, which could arise from the force of seaweed against ingestion. The parameter μ represents the endogenous excitation, that is, the tendency of neurons to fire spontaneously in the absence of motor inputs. The positive scaling constants ϵ and ζ control the magnitudes of the sensory feedback and the external load, respectively. In this thesis, we will set $\mathbf{l}(\mathbf{x})$ to a variety of constant values, so we subsume the parameter ζ into the external load henceforth. Specific parameter values are given in Appendix A.1. The roles of μ and ϵ are discussed further in Section 1.2.

The Shaw/Lytle model simplifies the anatomy of *Aplysia californica* to consider only the I2, I3, and I4 muscles (Fig. 1) and groups the neurons related to each muscle into three mutually inhibitory neural pools. The equations governing the neural dynamics are:

$$\begin{aligned}\frac{da_0}{dt} &= \frac{1}{\tau_a}(a_0(1 - a_0 - \gamma a_1) + \mu) + \epsilon(x_r - S_0)\sigma_0 \\ \frac{da_1}{dt} &= \frac{1}{\tau_a}(a_1(1 - a_1 - \gamma a_2) + \mu) + \epsilon(x_r - S_1)\sigma_1 \\ \frac{da_2}{dt} &= \frac{1}{\tau_a}(a_2(1 - a_2 - \gamma a_0) + \mu) + \epsilon(x_r - S_2)\sigma_2.\end{aligned}\tag{2}$$

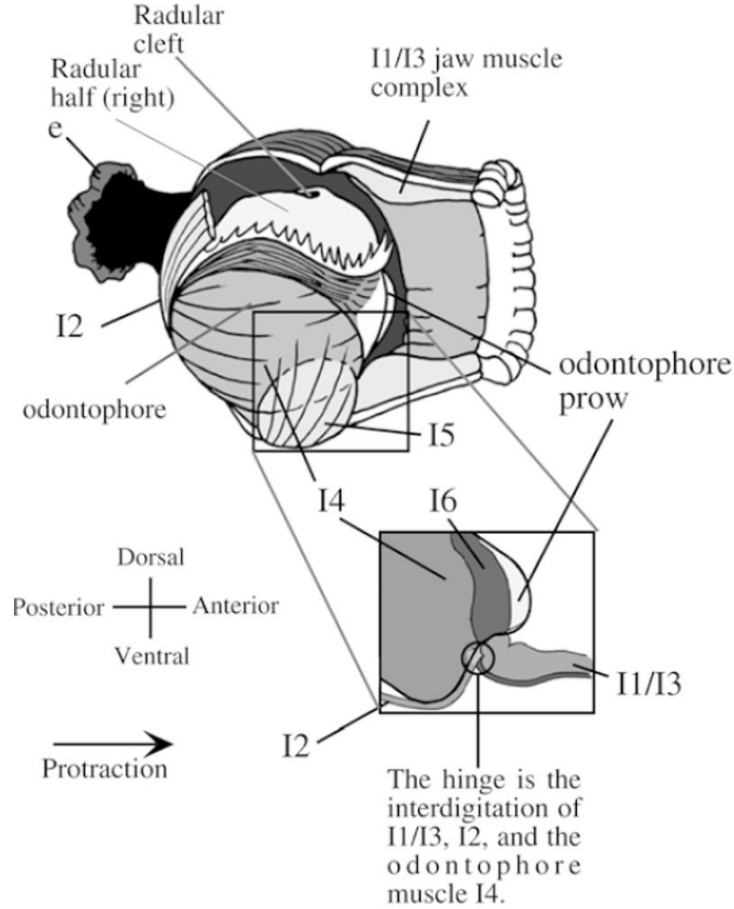


Fig. 1: Anatomy of the food grasping organ (also known as the radula/odontophore, or grasper) of *Aplysia californica*. The I2 muscle pushes the grasper forward to induce protraction. The I4 muscle induces the grasper to close. The squeezing of the I1/I3 muscle produces retraction. The remainder of anatomical details are not discussed in this thesis but can be found in [18]. Figure adapted (with permission) from Fig. 1 of [23].

The vector $\mathbf{a} = (a_0, a_1, a_2)$ represents the activity in the three neural pools. Neural pool a_0 corresponds to the B31, B32, B61, B62, and B63 neurons, and it is responsible for activating the I2 muscle which causes the grasper to protract. This motion is called the protraction phase. The a_1 neural pool represents the B31, B32, B61, B62, B63 and B8a, B8b [9] neuronal activities, and activates both the I2 and I4 muscles, which causes the grasper to close. These muscles push the seaweed away from the animal, which initiates the protraction-closed phase. The a_2 neural pool represents the B8a, B8b, B3, B6, and B9 neurons and the B64 interneuron.

Neurons B3, B6, B9, and B64 are responsible for activating the I3 retractor muscle. Together, the I3 and I4 muscles cause the grasper to retract while pulling in seaweed, and this motion is called the retraction phase. As shown in Fig. 2, oscillations in the neural pools generate oscillations in the periphery necessary for the slug to swallow seaweed.

In addition to the differential equations Eq. (2), the neural system is constrained by enforcing boundary conditions at a minimal and a maximal firing rate. Specifically, we require $1 \geq a_i \geq 0$ for each neural pool a_i . In our model, we have nonnegative levels of endogenous excitation ($\mu \geq 0$), which is always true for *Aplysia californica*. The boundary condition ensures that when $\mu > 0$, $\epsilon > 0$, or both, inhibition from sensory feedback does not result in negative neural activity ($0 > a_i$) or activity exceeding the maximum activation ($a_i > 1$).

Consider the neural dynamics at each face of the $[0, 1]^3$ space where $a_i = 0$ or $a_i = 1$ while $0 \leq a_j, a_k \leq 1$. Here we define a_j to be the neural pool that will fire after a_i , and a_k to be the previous neural pool. When there is no sensory feedback or endogenous excitation ($\mu = 0$ and $\epsilon = 0$), $\mathbf{a} \in [0, 1]^3$. Similarly, the trajectory is contained in the cube for nonzero endogenous excitation $\mu > 0$ and $a_i = 0$ because $\forall t, \frac{da_i}{dt} > 0$. However, if $\mu > 0$ and $a_i = 1$, the trajectory could exit the cube since $\frac{da_i}{dt} > 0$ when $\mu > \gamma a_j$. In addition, if there is sensory feedback ($\epsilon > 0$), a_i can also be driven negative and the trajectory could exit any face of the cube. Therefore, we impose hard boundary conditions on all sides of the unit cube, so the neural activations are contained in the invariant set $[0, 1]^3$, where 1 represents maximum activation and 0 is equivalent to quiescence.

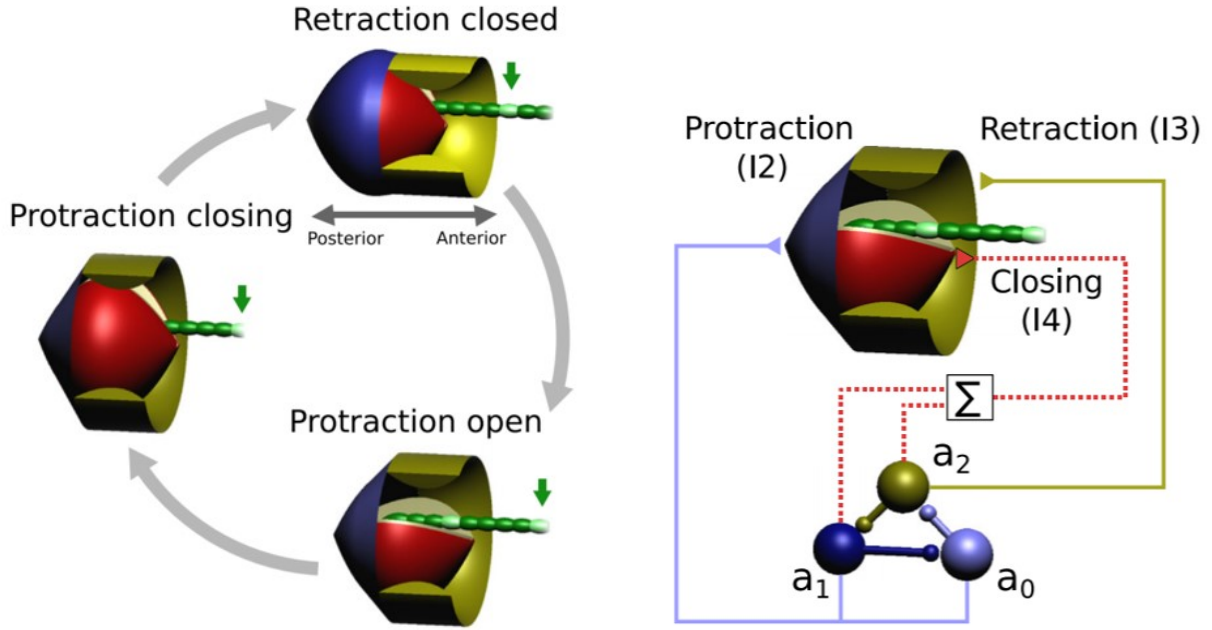


Fig. 2: Grasper motions and neural pools, from [22]. **Left:** The three phases of grasper motion with the green arrow indicating a specific point on the seaweed (green) being pulled in by the grasper with the I2 (blue), I4 (red), and I3 (yellow) muscles. **Right:** The mutually inhibitory neural pools are displayed with the activation of each neural pool corresponding to the recruitment and activation of a specific muscle. The left and right images corresponds to Shaw et al. [22] Fig. 2 and Fig. 3, respectively.

The neural dynamics are also regulated by different parameters, as well as the grasper position. Each neural pool receives proprioceptive feedback of the form $\epsilon(x_r - S_i)\sigma_i$. The position of the grasper is x_r , and the parameter S_i sets the proprioceptive neutral position for the i th neural pool. Parameter σ_i determines the direction of proprioceptive inputs to each neural pool relative to protraction versus retraction, and ϵ controls the overall strength of sensory feedback. The parameter τ_a is the neural pool time constant, and γ is the inhibition strength of the next neural pool. The mechanical advantage of each muscle will change depending on the position of the grasper [24]. As the equations above describe, sensory feedback influences the activity of each neural pool depending on the position of the grasper relative to the proprioceptive neutral positions. For example, when $x_r > S_0$, the position of the grasper extends past the proprioceptive neutral position of the I2 muscle and inhibits a_0

activity, whereas $x_r < S_0$ increases a_0 activity and causes the grasper to protract.

Using the same equations describing the muscle dynamics as [22, 13], we let the periphery incorporate activities from different neural pools to generate muscle activation:

$$\begin{aligned}\frac{du_0}{dt} &= \frac{1}{\tau_m} ((a_0 + a_1) u_{\max} - u_0) \\ \frac{du_1}{dt} &= \frac{1}{\tau_m} (a_2 u_{\max} - u_1).\end{aligned}\tag{3}$$

The state variable u_0 represents I2 muscle activity as a result of innervation from the a_0 and a_1 neural pools while the u_1 variable describes the I3 activity regulated by the a_2 pool. The parameter u_{\max} is the maximum muscle activation, and τ_m is the muscle activation time constant. The activities of the muscles in response to innervation from the nerves are slower compared to the acting neural pools. This phenomenon was previously described in an experimental study of *Aplysia* muscle [27], which the authors of the Shaw/Lyttle model [22, 13] used to derive the muscle activation dynamics.

The amount of force that muscles are able to produce depends on the length and direction in which they are stretched [28, 27]. Experimental studies of *Aplysia* feeding muscles showed nonlinear length-tension properties [27], which are similar to those assumed in [22, 13]. We describe the muscles generate force based on muscle activation and muscle position:

$$\begin{aligned}\phi(x) &= -\kappa x(x-1)(x+1) \\ F_{\text{musc}} &= k_0 \phi\left(\frac{x_r - c_0}{w_0}\right) u_0 + k_1 \phi\left(\frac{x_r - c_1}{w_1}\right) u_1\end{aligned}\tag{4}$$

The length-tension relationship of the muscle is described by the nonlinear function $\phi(x)$. Here a simplification to the biology is made so that the length-tension curve is described

by a cubic polynomial. The muscle force F_{musc} is the net force generated by the I2 and I3 muscles. The constant κ normalizes the maximum of the length-tension function to 1. I2 and I3 generate forces in opposite directions specified by k_0 and k_1 . The neutral positions for the I2 and I3 muscles are c_0 and c_1 . The parameters w_0 and w_1 are the maximal effective lengths of I2 and I3.

The state variables x_r and x_{sw} are the positions of the grasper and seaweed, respectively. The grasper position x_r oscillate within the range $[0, 1]$, where 0 is the anterior-most position and 1 is the grasper position during maximum protraction. An exception may occur where the grasper position exceeds 1 if the seaweed force overpowers the muscle force (Section 4.2). Acceleration is assumed to be insignificant, and b_r and b_{sw} are the damping parameters. The load F_{sw} is the resisting seaweed force. When the grasper is open, the Shaw/Lyttle model assumes that the grasper and seaweed do not interact [13, 22], so the seaweed position remains unchanged. The grasper position is a function of the muscle force when the grasper is open:

$$\begin{aligned}\frac{dx_r}{dt} &= \frac{F_{\text{musc}}}{b_r} \\ \frac{dx_{\text{sw}}}{dt} &= 0.\end{aligned}\tag{5}$$

However, when the grasper is closed, the grasper position is influenced by both the muscle force and seaweed force. Furthermore, both the grasper and the seaweed have the same rate of change in position:

$$\frac{dx_r}{dt} = \frac{dx_{\text{sw}}}{dt} = \frac{F_{\text{musc}} + F_{\text{sw}}}{b_r + b_{\text{sw}}}.\tag{6}$$

The grasper is defined to be closed when a_1 and a_2 activities exceeds a threshold (Section 1.3) and open otherwise. The parameters governing the opening and closing of the grasper will be the subject of our study.

1.2 Heteroclinic and Limit Cycle Regime

Limit cycles and heteroclinic orbits are special trajectories of continuous dynamical systems, defined as follows:

*“An isolated periodic trajectory is called a **limit cycle**. A limit cycle is said to be asymptotically stable if any [nearby] trajectory ... approaches the cycle as $t \rightarrow \infty$.”* [5].

*“A **heteroclinic orbit** corresponds to a trajectory that lies in both the unstable manifold of [one fixed point] and the stable manifold of [another fixed point].”* [2].

Furthermore, a limit cycle can also be *unstable*, if it repels at least some trajectories in any neighborhood of the periodic orbit, and the trajectory along a heteroclinic orbit approaches one fixed point as $t \rightarrow -\infty$ and the other as $t \rightarrow +\infty$. A sequence of heteroclinic orbits that form a closed loop is a *heteroclinic cycle* [20].

Recall from Section 1.1, the neural activity vector $\mathbf{a} = (a_0, a_1, a_2)$ is governed by Eq. (2). When $\epsilon = \mu = 0$, there are three saddle nodes at $(a_0, a_1, a_2) = (1, 0, 0)$, $(0, 1, 0)$, and $(0, 0, 1)$. These will be called the a_0 , a_1 , and a_2 *neural fixed points*, respectively. The heteroclinic orbit is an idealized trajectory that occurs when the endogenous activation is shut off ($\mu = 0$), the sensory feedback is absent ($\epsilon = 0$), and the inhibition is sufficiently strong ($\gamma > 2$). If $\mu \rightarrow 0$, then the trajectory approaches a heteroclinic cycle with an infinite “period” since the trajectory would take an infinite amount of time to travel from one fixed point to another.

Consequently, the rate of seaweed movement or the change in seaweed position per period ($\frac{\Delta x_{sw}}{\Delta t}$) will approach zero. We therefore assume the endogenous excitations are positive values, so the trajectory will only approach but not fall onto the heteroclinic orbit.

For different levels of endogenous excitation, Shaw et al. [22] divide trajectories into the heteroclinic regime ($\mu \lesssim 1.7 \times 10^{-5}$) and the limit cycle regime ($\mu \gtrsim 1.7 \times 10^{-5}$). As μ increases, the trajectories converge to limit cycles further away from the fixed points (Fig. 3). Consequently, the trajectories of the limit cycle regime spend less time near the fixed points compared to those in the heteroclinic regime. In contrast, trajectories generated from smaller μ values approach but do not come into contact with the fixed points. When $\mu \lesssim 1.7 \times 10^{-5}$, a longer retraction time was observed [13, 22] in comparison to the limit cycle regime, as the seaweed force was increased. Although oscillations in both the limit cycle regime and the heteroclinic regime are limit cycles, strictly speaking, they are divided into two distinct regions in the parameter space because the different ways that the trajectory interacts with the fixed points cause significant changes in the grasper behavior.

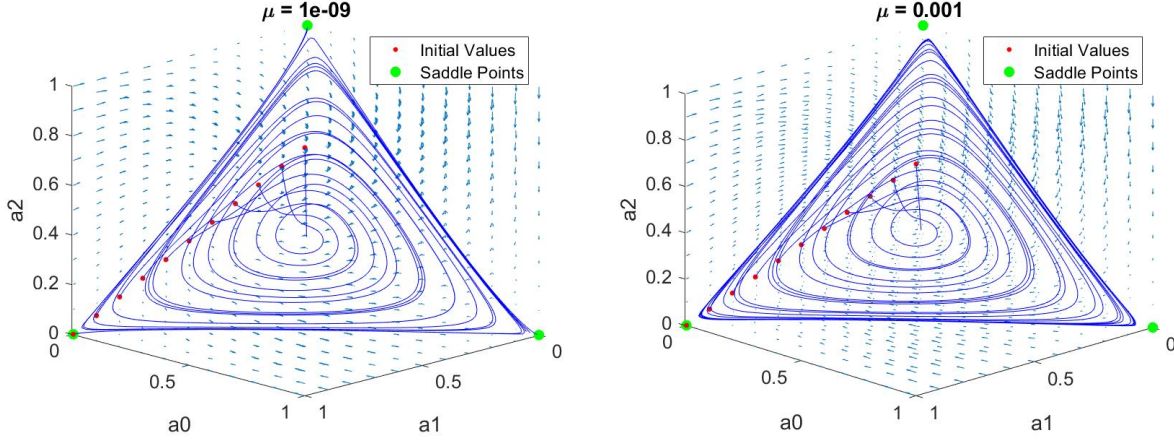


Fig. 3: Neural activation limit cycles from [22] in the absence of sensory feedback. The green dots represent the saddle fixed points corresponding to activation of the a_0 (bottom right), a_1 (bottom left), and a_2 (top) neural pools. **Left:** For small endogenous excitation ($\mu = 10^{-9}$), Eq. (2) produces a long-period limit cycle with trajectories (blue curves) that stay very close to the $\mu = 0$ heteroclinic cycle. **Right:** For larger excitation ($\mu = 10^{-3}$), the trajectories are steered further away from the fixed points. Both vector fields produce stable limit cycle trajectories because all trajectories in the state space converge to a limit cycle over time regardless of the initial conditions (red dots). Note that there is no sensory feedback in either system ($\epsilon = 0$).

Near the fixed points, the rate of change of the trajectory is the smallest (Fig. 3), and the role of sensory feedback becomes especially important. The perturbation ϵ may cause the system to escape the region near the fixed points faster. From Eq. (2), we can see that the greater the value of $|\epsilon - \mu|$ is, the greater the impact of perturbation; consequently, the heteroclinic regime with a smaller μ value is more responsive to sensory feedback [22]. In response to stronger seaweed force, the grasper in the heteroclinic regime increases the duration of the retraction phase. In contrast, the trajectories in the limit cycle regime, being less sensitive to sensory feedback, continue to perform the three phases of swallowing with much less change in behavior.

1.3 Measuring Fitness

In this thesis, we analyze the parametric sensitivity of Shaw and Lyttle’s *Aplysia californica* swallowing model [13, 22]. In these papers, the implicit goal of the feeding motor system is to ingest seaweed as rapidly as possible. Therefore, throughout this project, we choose our objective function S to be the average rate of seaweed intake:

$$S = - \lim_{t \rightarrow \infty} \frac{1}{t} \int_0^t \frac{dx_{sw}}{dt'} dt'. \quad (7)$$

The higher the average rate of seaweed intake, the higher the fitness. Under some conditions the model system loses seaweed, meaning $S < 0$. This situation might be interpreted as maladaptive behavior. Alternatively, under some experimental conditions *Aplysia* may be induced to reject inedible “food” [19, 17] in which case $S < 0$ could be interpreted as successful rejection behavior.

When a trajectory has converged to a stable limit cycle and the seaweed force is constant, the grasper behavior is identical between each period:

$$\begin{aligned} S &= - \lim_{n \rightarrow \infty} \frac{1}{n \cdot T} \int_0^{n \cdot T} \frac{dx_{sw}}{dt'} dt' \\ &= - \lim_{n \rightarrow \infty} \frac{n}{n \cdot T} \int_0^T \frac{dx_{sw}}{dt'} dt' = - \frac{1}{T} \int_0^T \frac{dx_{sw}}{dt'} dt' \end{aligned} \quad (8)$$

During each period, the grasper is open and closed in fixed time intervals. The Shaw/Lyttle model defined the grasper to be closed when

$$a_1 + a_2 \geq 0.5 \quad (9)$$

and open for all other values of a_1 and a_2 . Let $t_{\text{closed}} \in [0, T]$ be the first moment when the grasper closes and t_{open} , with $t_{\text{closed}} < t_{\text{open}} < t_{\text{closed}} + T$, be the time when the grasper transitions from closed to open. The objective function S can then be calculated using a smaller time window:

$$\begin{aligned} S &= -\frac{1}{T} \left(\int_{t_{\text{closed}}}^{t_{\text{open}}} \frac{dx_{\text{sw}}}{dt'} dt' + \int_{t_{\text{open}}}^{t_{\text{closed}}} \frac{dx_{\text{sw}}}{dt'} dt' \right) \\ &= -\frac{1}{T} \int_{t_{\text{closed}}}^{t_{\text{open}}} \frac{dx_{\text{sw}}}{dt'} dt' = -\frac{x_{\text{sw}}(t_{\text{open}}) - x_{\text{sw}}(t_{\text{closed}})}{T}. \end{aligned} \tag{10}$$

Recall the integral from t_{open} to t_{closed} is identically zero because the model assumes the seaweed does not move while the grasper is open.

We will analyze the parametric sensitivity of the system by exploring the effects of varying different parameters in the heteroclinic regime at a fixed level of endogenous excitation (specifically, $\mu = 10^{-6}$). We redefine the parameterization of the grasper-open and grasper-closed regions (cf. Eq. (9)) and describe how we implement our model in Chapter 2. In Chapter 3, we measure the change in fitness and observe different ingestion and egestion behaviors in different parameter regions. We then investigate the robustness of the feeding system by examining the effect of varying the load in the different regions in Chapter 4.

2 Sensitivity to Opening/Closing Boundary

In this chapter, we explain our methodology for evaluating our objective function S (Section 1.3, Eq. (10)) which measures the rate of seaweed movement over different parameterizations of grasper behavior. Our project builds on a simulation of the Shaw/Lyttle model implemented in Matlab by Dr. Yangyang Wang [13, 22]. We introduce alternative parametrizations of the switching surface defining the opening/closing threshold in Section 2.1. We explain our implementation of the model in Section 2.2.

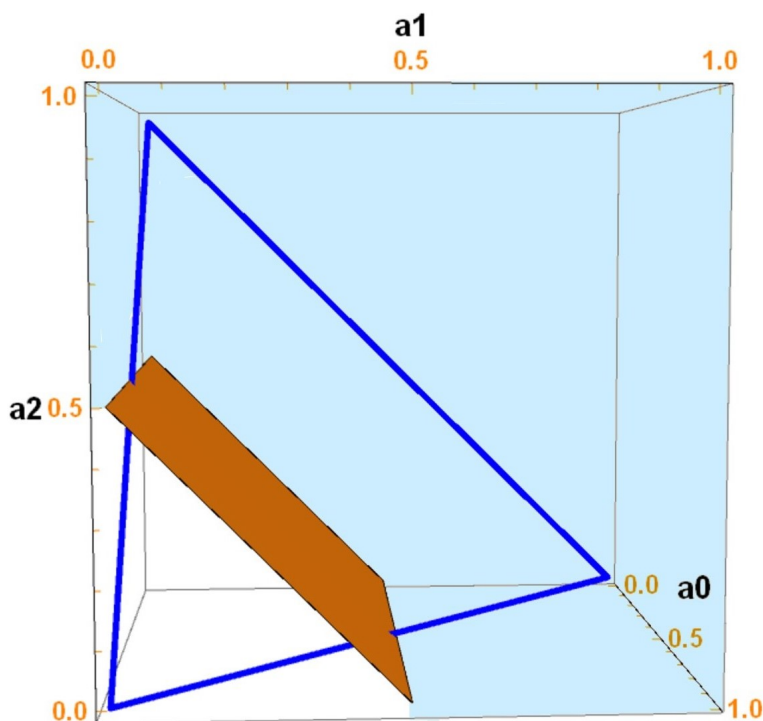


Fig. 4: Grasper-open and grasper-closed regions. Heteroclinic orbit (blue, $\mu = 0$) intersected by a plane (orange) dividing the trajectory traveling counterclockwise into grasper-open (unshaded) and grasper-closed (shaded) regions. The points $(a_1, a_2, a_3) = (1, 0, 0)$, $(0, 1, 0)$, and $(0, 0, 1)$ are the fixed points for the three neural pools.

The Shaw/Lyttle model divides the neural activity space into grasper-open and grasper-closed regions according to Eq. (9), as Fig. 4 illustrates. This figure contains a heteroclinic orbit which arises when there is no endogenous excitation ($\mu = 0$) and sensory feedback

($\epsilon = 0$). However, we are interested in trajectories in the heteroclinic regime (specifically, $\mu = 10^{-6}$) where the neural oscillations approach but do not contact the fixed points, much like the graphs shown in Fig. 3. Once the trajectories have converged to a stable orbit, the sum of the three neural activities is approximately 1 [13]. Thus, in Figs. 5 and 6 we plot the trajectory and the opening/closing boundary in the (a_1, a_2) -plane, and note that $a_0 \approx 1 - a_1 - a_2$.

2.1 Parameterizing the Open and Closed Regions

We wish to write the grasper closing condition Eq. (9) in a more general form. We will assume the grasper is closed whenever the activations of the neural pools satisfy the following inequality:

$$\beta \cdot a_1 + \gamma \cdot a_2 \geq \delta. \quad (11)$$

The grasper is open for all other combinations of a_1 and a_2 . If $\beta = \gamma = 1$ and the closing threshold is $\delta = 0.5$, the new parameterization is equivalent to the original condition (Eq. (9)) from the Shaw/Lyttle model. This new parameterization allows us to explore how variations in a_1 and a_2 activities affect the opening and closing of the grasper.

Alternatively, we may transform the parameterization from Eq. (11) into a more illuminating expression that will allow us to systematically vary the closing condition. Let L be the line of equality dividing the opening and closing regions in the (a_1, a_2) -plane:

$$L = \{(a_1, a_2) \mid a_2 = -\frac{\beta}{\gamma} \cdot a_1 + \frac{\delta}{\gamma}\}. \quad (12)$$

Define P to be the line perpendicular to L that intersects the point $(a_1, a_2) = (0, 0)$. P is

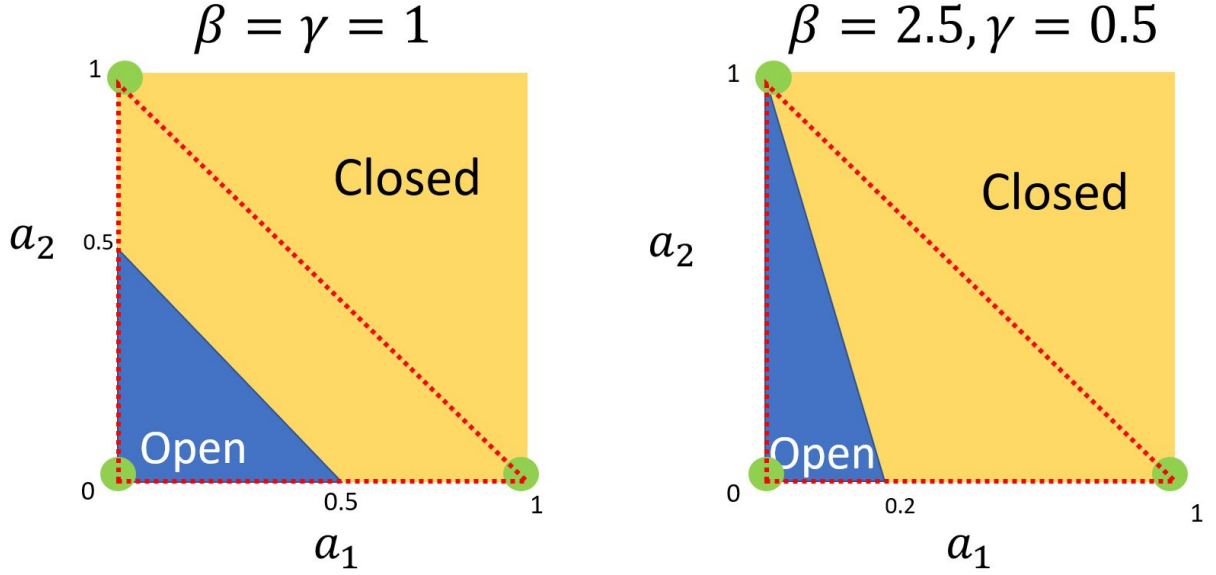


Fig. 5: Grasper-open and grasper-closed regions parameterized by β and γ . The a_0 , a_1 , and a_2 fixed points (green) are located at positions $(0, 0)$, $(1, 0)$, and $(0, 1)$ in the (a_1, a_2) -plane. The red, dashed line represents the trajectory, moving counterclockwise. **Left:** Projection of the neural activity using the original parameters from [22], i.e. $\beta = \gamma = 1$. **Right:** Projection of the neural activity using $\beta = 2.5$ and $\gamma = 0.5$. In both panels, $\delta = 0.5$.

thus the line:

$$P = \{(a_1, a_2) \mid a_2 = \frac{\gamma}{\beta} a_1\}. \quad (13)$$

Define a positive constant $z = \sqrt{\beta^2 + \gamma^2}$. Then, we can re-parameterize inequality (11) as:

$$\frac{\beta}{z} \cdot a_1 + \frac{\gamma}{z} \cdot a_2 \geq \frac{\delta}{z}. \quad (14)$$

The coefficients from (14) can be rewritten as:

$$\begin{aligned} \cos(\theta) &= \frac{\beta}{z} \\ \sin(\theta) &= \frac{\gamma}{z} \\ C &= \frac{\delta}{z}. \end{aligned} \quad (15)$$

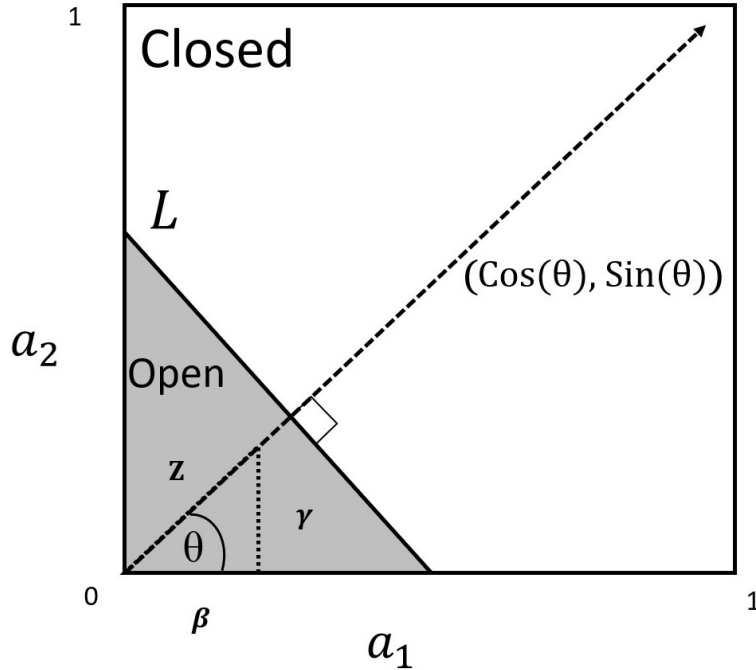


Fig. 6: Defining different opening (gray) and closing (white) regions using an orthogonal vector $(\cos(\theta), \sin(\theta))$. The vector (dashed) normal to the boundary (L) dividing opening and closing regions is derived using the neural pool weighting parameters β and γ as well as the threshold δ , which corresponds to the a_2 -intercept. This vector forms angle θ with the a_1 -axis.

Where θ is the angle between P and the a_1 -axis. We can now transform the original inequality into the final expression:

$$\cos(\theta) \cdot a_1 + \sin(\theta) \cdot a_2 \geq C. \quad (16)$$

The vector $(\cos(\theta), \sin(\theta))$ is orthogonal to the boundary L dividing the opening and closing regions. Fig. 6 illustrates the construction of expression (16).

The closing condition in the Shaw/Lyttle model is defined by $\beta = \gamma = 1$ and $\delta = 0.5$, giving $1 \cdot a_1 + 1 \cdot a_2 = \delta$, so the original condition is equivalent to expression (16) with $\theta = \frac{\pi}{4}$. We

re-parameterize to find the threshold δ :

$$\begin{aligned}
C &= \cos(\theta) \cdot a_1 + \sin(\theta) \cdot a_2 \\
&= \cos\left(\frac{\pi}{4}\right) \cdot a_1 + \sin\left(\frac{\pi}{4}\right) \cdot a_2 \\
&= \frac{\sqrt{2}}{2} \cdot (a_1 + a_2) = \frac{\sqrt{2}}{2} \cdot \delta \\
&= \frac{\delta}{\sqrt{2}}
\end{aligned}$$

or equivalently:

$$\delta = C \cdot \sqrt{2}.$$

Thus, by varying $\theta \in [0, 2\pi]$ and $\delta \in \mathbb{R}$, we can define all possible geometries for the open and closed regions.

2.2 Model Implementation

In order to study the parametric sensitivity of *Aplysia californica*'s grasper behavior, we adapted a Matlab implementation of the Shaw/Lyttle model written by Dr. Yangyang Wang [25]. As Dr. Wang's code was not intended to facilitate parametric sensitivity studies, we modified the code to introduce parameters θ and δ controlling the opening/closing surface.

The Matlab differential equations solver ODE15s evaluates the seven state variables: $a_0, a_1, a_2, u_0, u_1, x_r$, and x_{sw} . This numerical integration function is applied with Relative Tolerance = Absolute Tolerance = 10^{-13} and the maximum step size = 10^{-3} . The parameters are identical to the values used by Lyttle et al. [13] except for the following: the endogenous excitation ($\mu = 10^{-6}$), the sensory feedback ($\epsilon = 10^{-4}$), and seaweed force ($F_{sw} = 0.1$). See Tables 1 and 2 for initial conditions and parameter values, respectively (Appendix A.1). In this

thesis, we will investigate trajectories in the heteroclinic regime (cf. Section 1.2 for more information).

Using the Matlab solver and specifications given in the paragraph above, Dr. Wang's original code (`lyttle_model.m`, Appendix A.2) produces Fig. 7, where the four panels represent the trajectories for neural pool activities, muscle activities, grasper position, or seaweed position. In Fig. 7A, which plots the neural activity variables, one can see the difference in duration of neural activity due to the influence of sensory feedback. Both the a_0 and a_1 neural pools innervate the I2 protractor muscle. The onset of the a_0 activity pushes the grasper away from the I2 proprioceptive neutral position, so the ensuing a_1 pool activity is met with inhibition due to sensory feedback (Eq. (2)). All brain/body variables (a_0 , a_1 , a_2 in Fig. 7A, u_0 , u_1 in Fig. 7B, and x_r in Fig. 7C) have periodic trajectories. The only non-periodic state variable is the seaweed position (Fig. 7D). However, once the trajectory has converged to a stable limit cycle, the rate of change of the seaweed position is periodic. As described in Section 1.1, the grasper has three different motions thereby producing three distinct types of seaweed movement. When the grasper is in the protraction-open phase, the grasper is not in contact with the seaweed, so the seaweed position does not change. In the protraction-closed phase, the seaweed is pushed away from the slug (positive change in position, see Fig. 7D). The seaweed is ingested during the retraction-closed phase of the grasper (negative rate of change, see Fig. 7D).

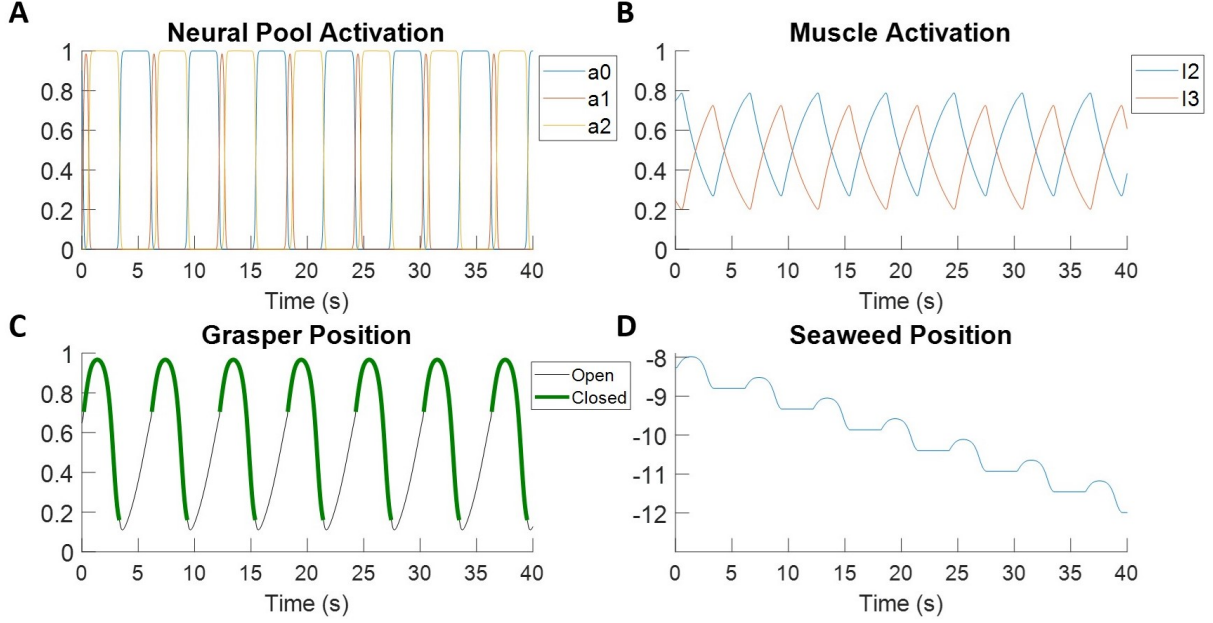


Fig. 7: Evolution of state variables of the Shaw/Lyttle model. Parameters as in Table 1 of [13], with $\mu = 10^{-6}$. Plots generated using Dr. Yangyang Wang’s Matlab simulation. **(A)** Neural activity, showing a near-heteroclinic trajectory, with long activations for a_0 and a_2 neural pools and short activation for the a_1 pool. **(B)** Periodic muscle activity of the u_0 and u_1 variables corresponding to the I2 and I3 muscle groups, respectively. **(C)** Oscillating grasper position with negative and positive slopes representing retraction and protraction, respectively. **(D)** Negative change in seaweed position corresponds to ingestion (seaweed movement into the slug). The seaweed position is assumed to be fixed when the grasper is open. The brief a_1 activity causes some loss of seaweed, resulting in short positive changes in the seaweed position.

Recall from Section 1.3, Eq. (7), that

$$S = - \lim_{t \rightarrow \infty} \frac{1}{t} \int_0^t \frac{dx_{sw}}{dt'} dt' = - \frac{x_{sw}(t_{open}) - x_{sw}(t_{closed})}{T}.$$

To accurately measure the average rate of seaweed movement, suppose the first point of measurement is at $x_{sw}(t_0)$ ($t_0 \approx 15$ in Fig. 8) and the ensuing points are measured at $x_{sw}(t_0 + n \cdot T)$, where $n \in \mathbb{N}$ and T is the period. Since the trajectories have converged to a limit cycle, the net seaweed displacement per period is approximately constant. Therefore, the seaweed intake rate can be estimated as the net change in seaweed position between the

first and last point divided by the elapsed time:

$$S \approx -\frac{x_{\text{sw}}(t_0 + \rho \cdot T) - x_{\text{sw}}(t_0)}{\rho \cdot T},$$

$$\rho = \max_{n \in \mathbb{N}} \left(n \leq \frac{40 - t_0}{T} \right).$$
(17)

The simulation time is 40 seconds, and the first 10 seconds of activity are discarded as transient under the assumption that 10 seconds is enough time for the limit cycle to converge to stable orbit (Fig. 8).

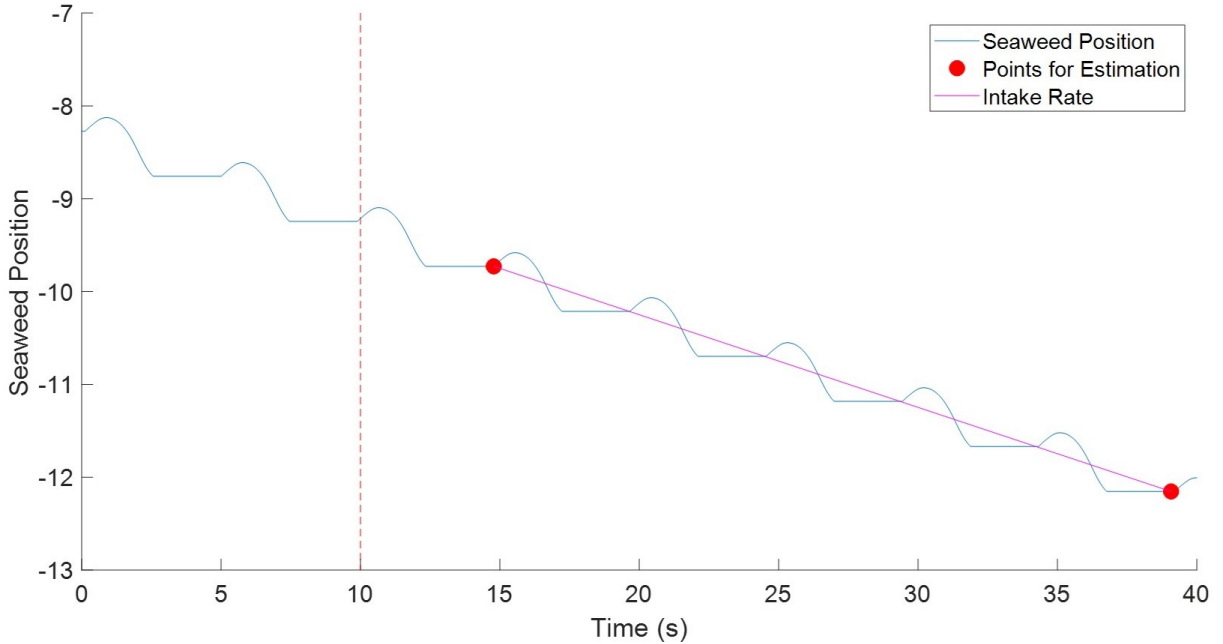


Fig. 8: Measurement of S , the rate of seaweed intake. Values to the left of the dashed red line are discarded as the initial transient. The ingestion rate is measured between corresponding points for each periodic motion of the seaweed position, divided by the total time elapsed. The slope of the pink line gives (-1) times the average rate of seaweed movement (S).

Points of measurement are taken when the seaweed velocity changes from 0 to a nonzero value. Thus, each measurement point corresponds to a crossing from the grasper-open region into the grasper-closed region. In Fig. 8, these points occur when the seaweed position changes from flat to rising. However, in some combinations of θ , δ , and F_{musc} could also be

measured when the seaweed position changes from flat to falling.

We apply a different convention concerning the direction of seaweed movement than what is used in the Shaw/Lyttle model [22, 13]. In the Shaw/Lyttle model, negative change in seaweed position corresponds to ingestion while positive change represents to egestion. However for this thesis, positive average rate of seaweed movement ($S > 0$) represents ingestion while negative rate ($S < 0$) is egestion. When graphing seaweed position, we will revert back to the original Shaw/Lyttle convention for easier comparison of the result with that of the original papers [13, 22], cf. Figs. 7, 8, 16, 15, and 17.

Utilizing the parameterization from the previous section, and varying θ and δ to define different open and closed regions (Eq. (16), Section 2.2), we measure intake rates produced by $\theta \in [0, 2\pi]$ and $\delta \in [-0.5, 1.5]$ by applying the Matlab codes given in Appendix A.2. We systematically vary the angle and threshold (`lyttle_model_vary_grasper_run.m`) and evaluate the corresponding trajectory using the code in (`lyttle_model_vary_grasper.m`)¹. We numerically estimate fitness, following the procedure described in the paragraph above (`lyttle_model_vary_grasper_run.m`). To perform analysis using a specific combination of angle and threshold parameters, we visualize our result by plotting the evolution of the state variables

(`lyttle_model_state_var_plots.m`), compare neural fixed points captured in different grasper-closed regions (`RegionGeometry.m`), and explore how variations in load affect fitness (`Fsw_vsIntakeRate.m`)

Section 4.2 evaluates two trajectories at different seaweed forces but with the same parameterization of the grasper closing condition. The rate of divergence of the two trajectories were approximated and graphed

¹Dr. Peter Thomas wrote this file by modifying `lyttle_model.m`.

(Rate_of_change_of_differences_dzdt). We then compare grasper behaviors at different parameterizations using the same seaweed force (grasperForceCompare.m).

3 Grasper Behaviors in Distinct Parameter Regions

3.1 Identifying Parameter Regions

In this chapter, we explore the change in S , the average rate of seaweed movement, as a result of different parameterizations of the grasper closing conditions (Eq. (16)). By systematically varying angle ($\theta \in [0, 2\pi]$) and threshold ($\delta \in [-0.5, 1.5]$), we identified eight *parameter regions*, or sections in Fig. 9 with qualitatively distinct seaweed behaviors. Here, $0 < S$ means seaweed ingestion while $S < 0$ represents egestion. We indexed these non-overlapping regions with roman numerals such that if S_j is the average rate of seaweed movement where $j \in [\mathbf{I}, \mathbf{II}, \dots, \mathbf{VIII}]$, then $S_{\mathbf{I}} \geq S_{\mathbf{II}} \geq \dots \geq S_{\mathbf{VIII}}$.

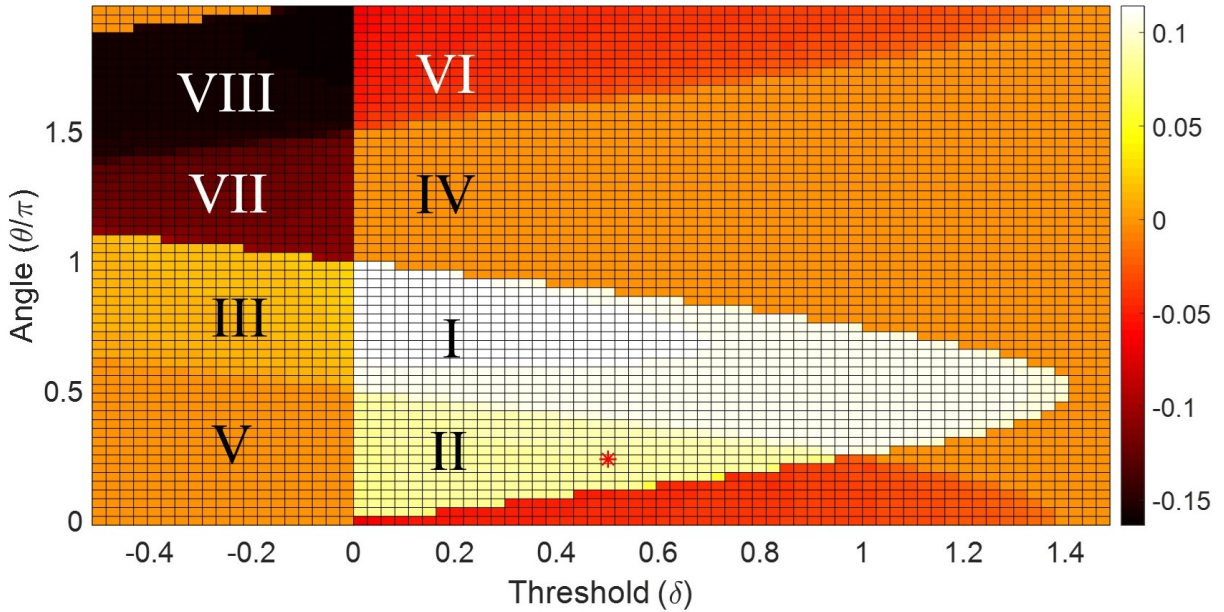


Fig. 9: Average rate of seaweed movement S evaluated at different values of the parameters governing the closing condition. This colormap is numbered according to the colorbar from regions with the greatest average rate of seaweed movement (**I**) to the lowest (**VIII**). Here, positive rate refers to ingestion, and negative values represent egestion. Although regions **IV** and **V** both have $S = 0$, the grasper behaviors between each region are distinct (cf. Section 3.2). These two regions are separated by the line $\delta = 0$. The angles are discretized into 60 equally spaced points and the threshold into 75. The red asterisk approximate the parameters used in [13, 22].

Each region is classified into one of three types: intake, neutral, or rejection. The *intake regions* contain all parameter combinations that produce ingestion of seaweed ($S > 0$): regions **I**, **II**, and **III**. The closing condition used by the Shaw/Lyttle model ($\delta = 0.5, \theta = \pi/4$, cf. Eq. (9)) lies in region **II** (red asterisk in Fig. 9). There are two distinct *neutral regions* that produce no net seaweed movement ($S = 0$): regions **IV** and **V**. Although these regions appear indistinguishable in Fig. 9, they are separated by the $\delta = 0$ line, and the grasper behaves differently in each region (cf. Section 3.3). The grasper in the *rejection regions* ejects or loses seaweed every period ($S < 0$) and include: regions **VI**, **VII**, and **VIII**. In Section 3.3 we will analyze the grasper behaviors in each region. The distribution of the rates of seaweed movement across different parameterizations are shown in Fig. 10.

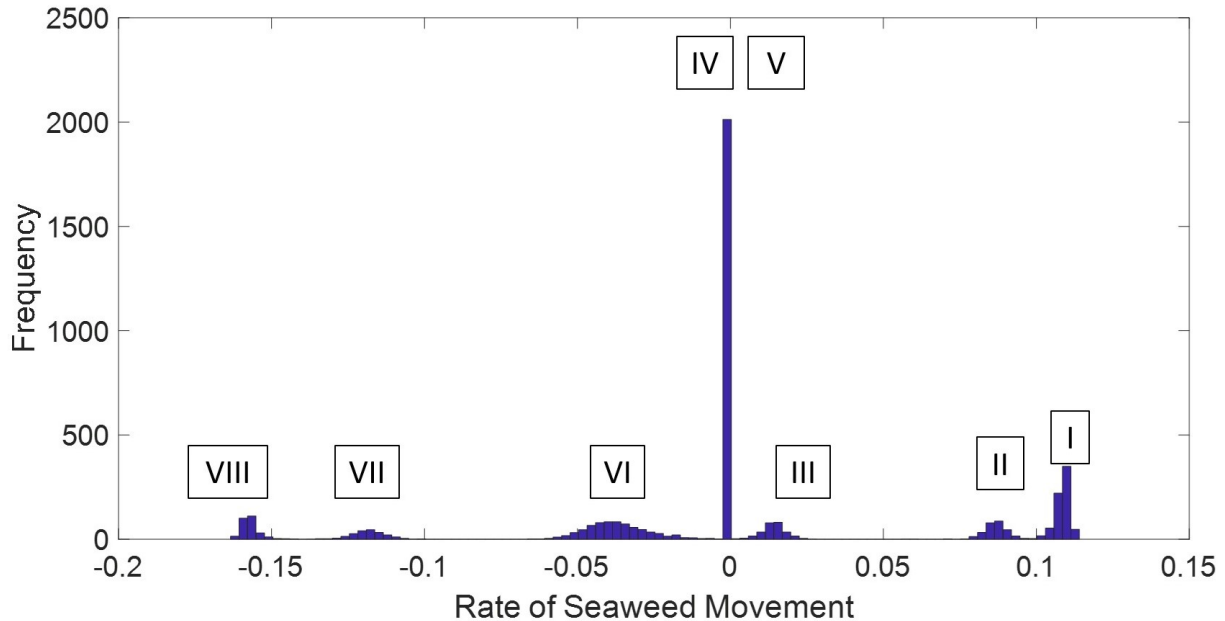


Fig. 10: Distribution of seaweed rates across the 60×75 grid containing different combinations of angle and threshold. Average rates of seaweed movement can be classified into seven groups and correspond to the eight parameter regions in Fig. 9.

3.2 Fixed Points Distinguish Parameter Regions

To begin understanding each parameter region, we identify the switching boundary in the (a_1, a_2) -plane and analyze how the grasper-open and grasper-closed regions are divided (refer to Section 2.1 for additional background information). Fig. 11 illustrates the threshold locations in (a_1, a_2) coordinate space for selected points in the (δ, θ) parameter plane (cf. Fig. 14).

We observe that each of the regions includes a different set of neural fixed points, or equilibrium points, in its grasper-closed space. Recall from Section 1.2 that the rate of change of neural vector \mathbf{a} is slowest near the neural fixed points. Therefore, having a fixed point captured in the grasper-closed region results in sustained stimulation of the muscle driven by the neural pool, which then develops a significant force on the seaweed. The a_2 unit is the only neural pool that drives the I3 muscle and grasper retraction, and all three intake regions capture the a_2 fixed point. The rejection regions include either the a_1 fixed point (region **VI**), a_0 fixed point (region **VII**), or both (region **VIII**). Both the a_0 and a_1 neural pools drive the I2 muscle that causes grasper protraction. Parameter region **IV** excludes all fixed points, so the grasper is always open; therefore in the model, the instantaneous rate of movement of seaweed is identically zero at all times. In contrast, region **V** includes every fixed point, so the grasper always remains closed, and pulls the seaweed back and forth with no net ingestive or egestive movement. Thus, the different rates of seaweed intake may be explained by the specific neural fixed points included in the grasper-closed region.

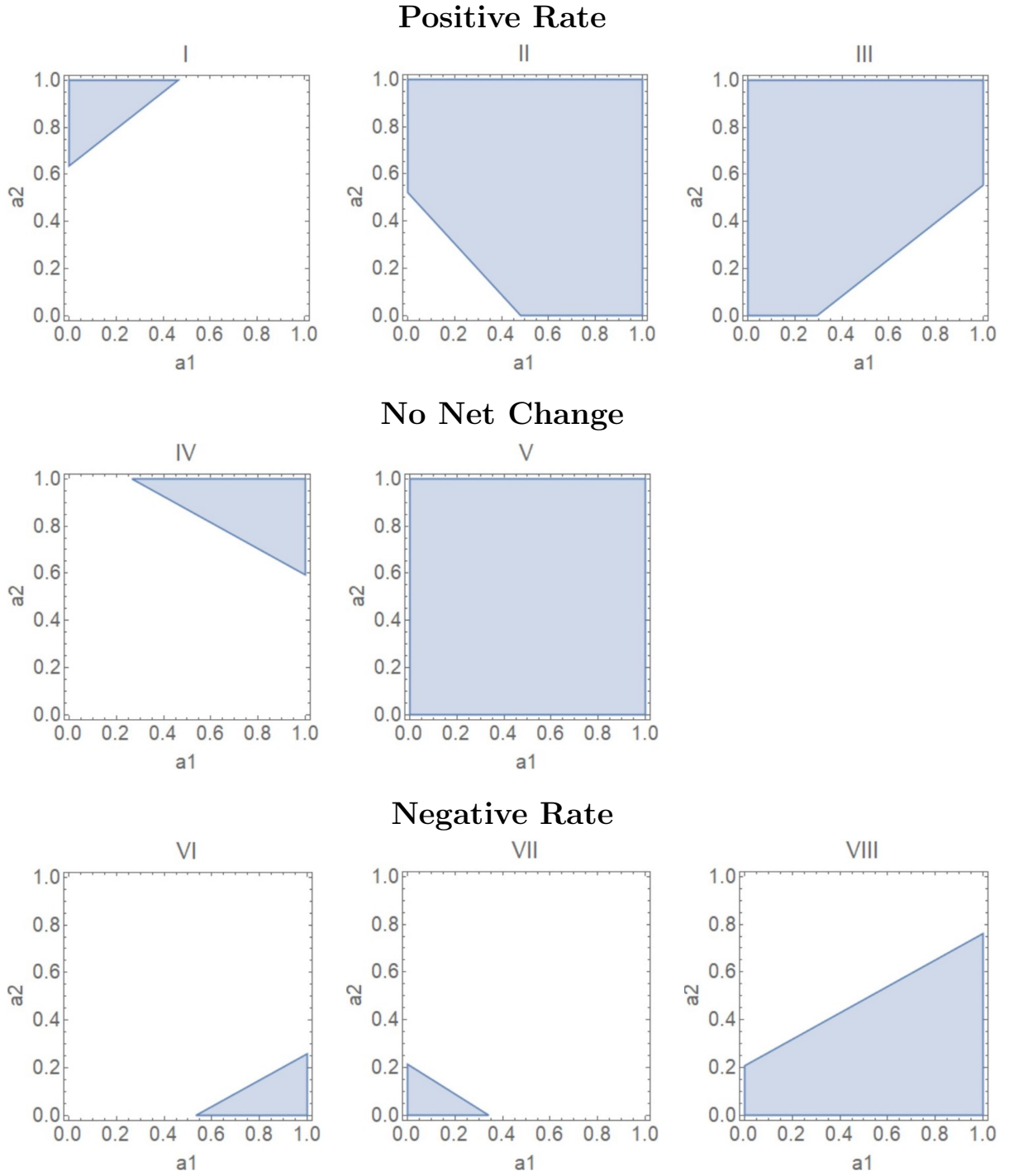


Fig. 11: Switching boundary in different parameter regions. The eight parameter regions are divided into three groups depending on the direction of seaweed movement per period. From top to bottom, the three groups correspond to intake, neutral, and rejection regions. In each panel, the shaded and unshaded regions correspond to grasper-closed and grasper-open spaces, respectively.

To verify whether the previous observation can be generalized to all angle-threshold combinations, we investigate the distribution of fixed points encompassed by the grasped-closed space of all parameter regions. For each (δ, θ) , we determine which of the fixed points $(a_1, a_2) \in \{(0,0), (0,1), (1,0)\}$ satisfy the closing condition (Eq. (16)). Fig. 12 shows the resulting map, with distinct *fixed point regions*, areas that capture a specific set of fixed points.

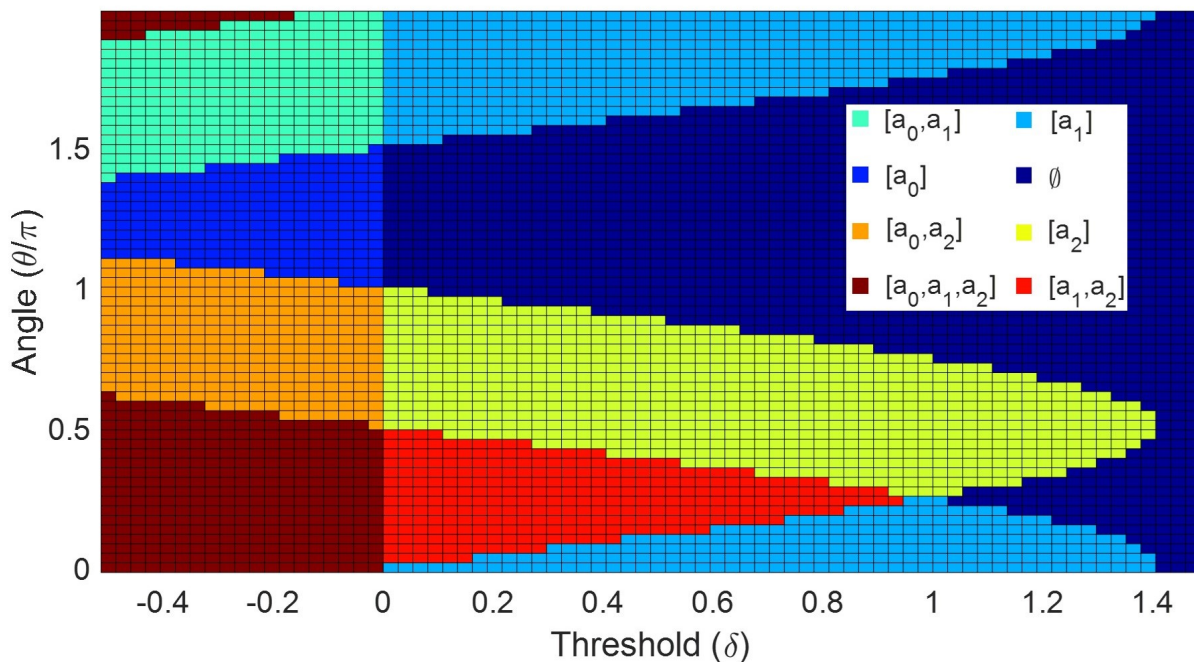


Fig. 12: Different neural fixed points satisfy varying parameterizations of the grasped closing condition. Regions of the same color encompass the same set of fixed points in the grasped-closed space. The only part of the graph with no fixed points included within its grasped-closed region is the area in dark blue.

The distribution of the different regions appear to be similar to those of Fig. 9.

To understand the relationship between the neural fixed points and the parameter regions, we derive the boundaries between the fixed point regions explicitly. Recall that the grasped-

closed condition is defined by Eqs. (16) and (17) as:

$$\cos(\theta) \cdot a_1 + \sin(\theta) \cdot a_2 \geq \frac{\delta}{\sqrt{2}} \quad (18)$$

The boundaries divide the regions including different fixed points clearly. Regions with the a_0 fixed point in the closed region obey the following:

$$0 \geq \frac{\delta}{\sqrt{2}} \quad (19)$$

The regions where closing includes the a_1 fixed point satisfy:

$$\cos(\theta) \geq \frac{\delta}{\sqrt{2}} \quad (20)$$

The regions where closing includes the a_2 fixed point satisfy:

$$\sin(\theta) \geq \frac{\delta}{\sqrt{2}} \quad (21)$$

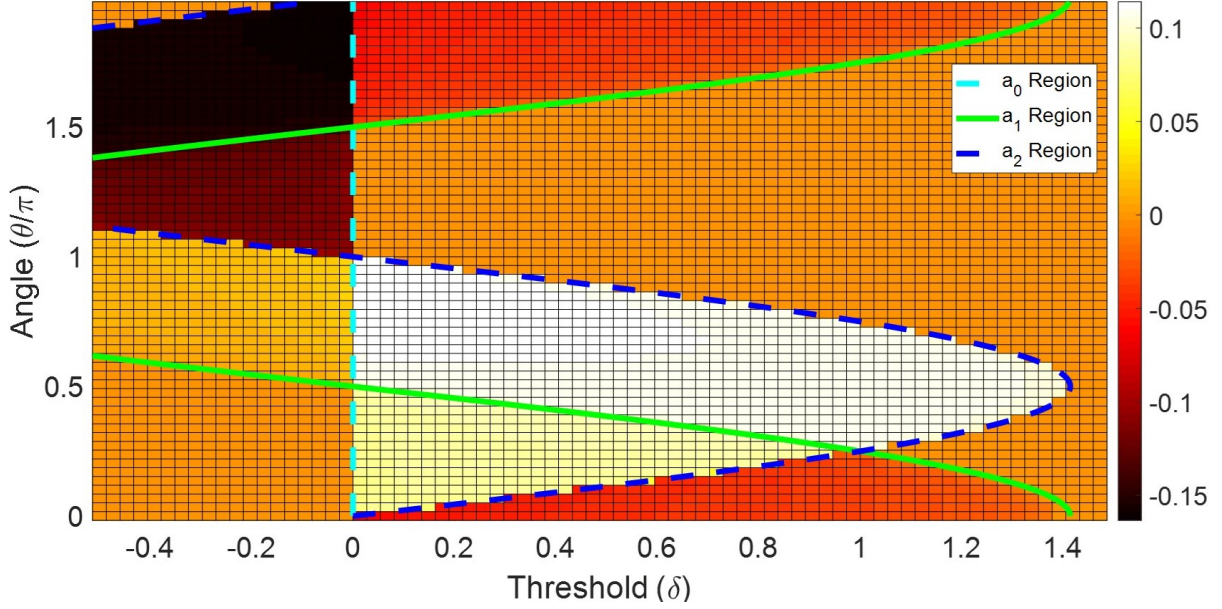


Fig. 13: Comparison between the parameter regions and the fixed point regions. The a_0 , a_1 , and a_2 fixed point boundaries outline the eight different fixed point regions corresponding to $0 \geq \frac{\delta}{\sqrt{2}}$, $\cos(\theta) \geq \frac{\delta}{\sqrt{2}}$, and $\sin(\theta) \geq \frac{\delta}{\sqrt{2}}$, respectively. These boundaries are also the boundaries of the intake regions.

To see how fixed points affect S , we overlay the boundaries dividing the fixed point regions on top of the parameter regions in Fig. 13. These boundaries are indistinguishable from the curves dividing the parameter space into the eight regions; that is to say, the parameter and fixed point regions overlap. Therefore, knowing which fixed points are included in the grasped space allows us to predict the average rate of seaweed movement. The next section will discuss how the fixed points affect the grasped and seaweed movement in more detail.

3.3 Analyzing the Parameter Regions

At the end of Section 3.2, we established that the neural fixed points in the grasped space affect the average rate of seaweed movement, and points in the same parameter region

share the same neural fixed points. Therefore, we selected one (δ, θ) point as representative from each parameter region to analyze the variations in S . The points selected are shown in Fig. 14.

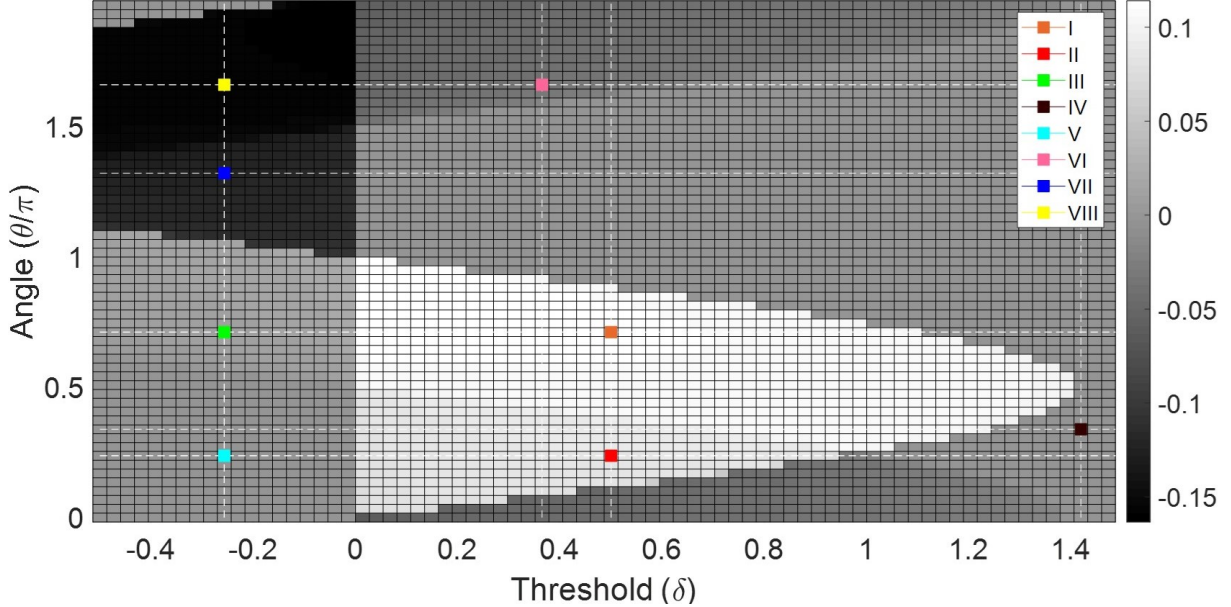


Fig. 14: Points are selected from each of the eight parameter regions. The red point from region **II** is closest to the angle and threshold values used by Shaw et al. [22]. The points have the following $(\delta, \frac{\theta}{\pi})$ coordinates. **I**: (0.5, 0.7119), **II**: (0.5, 0.2373), **III**: (0.2568, -0.7119), **IV**: (1.4189, 0.3390), **V**: (-0.2568, 0.2373), **VI**: (0.3649, 1.661), **VII**: (-0.2568, 1.322), **VIII**: (-0.2568, 1.661).

The red point in region **II** $((\delta, \theta) = (0.5, 0.2373\pi))$ corresponds to the parameters closest to those used in (Eq. (9)) in the Shaw/Lyttle model $((\delta, \theta) = (0.5, 0.25\pi))$. These selected values will be used throughout the remainder of the thesis.

From Section 3.1, we classified the parameter regions into three groups: intake, neutral, and rejection regions (Fig. 11). Region **I** has the highest fitness out of all the regions, and its grasper-closed region captures only the a_2 fixed point, thus ensuring that the grasper is only closed during retraction (Figs. 15). Region **II** has parameters closest to the ones used in the original model [13, 22]. The closing condition from this region includes the a_2 and a_1 fixed

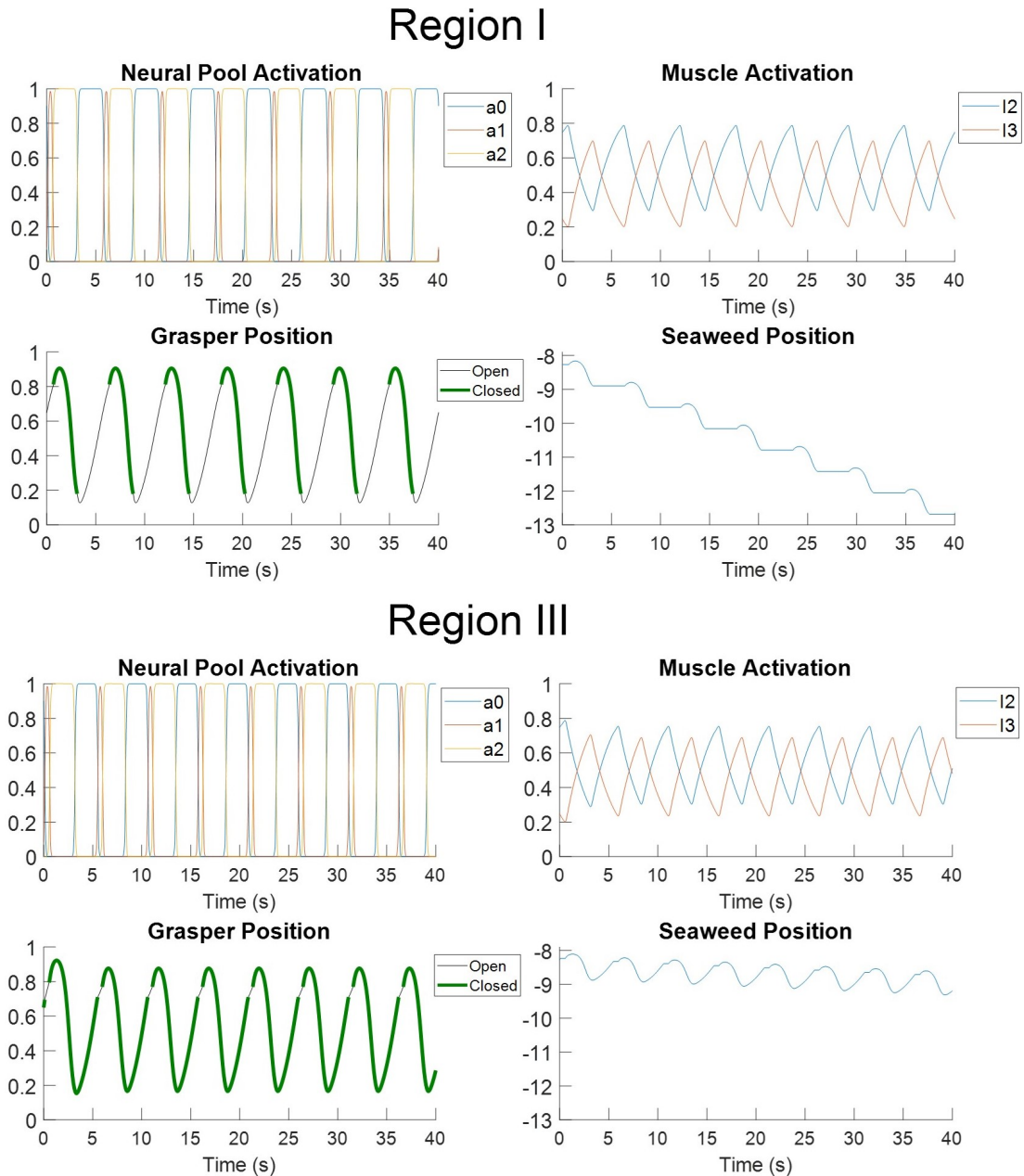


Fig. 15: Evolution of state variables from the intake regions **I-III**. In the neural pools and muscle activities, positive values represent higher activation. The negative change in grasper and seaweed positions represent retraction, i.e. movement into the slug. Region **II** has a lower intake rate than region **I** ($S_I > S_{II}$). Trajectories in region **II** (not shown) are qualitatively similar to those in region **I**, except for a longer protraction-closed phase, shown as positive seaweed movement resulting in seaweed loss.

points to produce the protraction-open, protraction-closed, and retraction-closed behaviors described in Section 1.1. Changes in seaweed position in regions **I** and **II** are qualitatively similar. However, **I** has a shorter protraction closed phase which reduces the loss of seaweed

per period.

Region **III** shows the smallest positive intake rate because both the a_2 and a_0 fixed points satisfy the closing condition. In this region, the grasper is closed during retraction, as well as during part of the protraction phase, which results in lower ingestion rate than the regions above. Because the grasper is closed near a_0 in region **II**, instead of a_1 in **III**, we observe that $S_{\text{II}} > S_{\text{III}}$. The trajectory passes by the a_0 fixed point more slowly than the a_1 fixed point due to the grasper's response to feedback; this phenomenon was also observed by Shaw et al. [22]. As a result, even though both the a_0 and a_1 neural pools innervate the I2 protractor muscle, a_0 is active for a longer duration than a_1 , so more seaweed is ingested during the part of the trajectory that passes by the a_0 point than the part passing by the a_1 point.

Although $S = 0$ in both neutral regions, regions **IV** and **V** have very different grasper and seaweed movements (Figs. 16). In region **IV**, the grasper-closed space does not overlap with any part of the trajectory, so the grasper is always open. Because we assumed that the seaweed position is fixed when the grasper is open, there is no change in seaweed position. In contrast, the trajectory always satisfy the closing condition in region **V**. Therefore, the grasper is always closed, and the seaweed oscillates back and forth along with the grasper with no net change in position.

In contrast to the behavior in the ingestive regions, when the parameters fall in the rejection regions (**VI-VIII**), the grasper closes during protraction and opens during retraction. Consequently, seaweed is ejected from the slug, resulting in egestion (Fig. 17). This behavior differs from the swallowing behavior (protraction-open, protraction-closed, and retraction) studied in [13, 22]. The closing condition of regions **VI**, **VII**, and **VIII** includes the a_1 ,

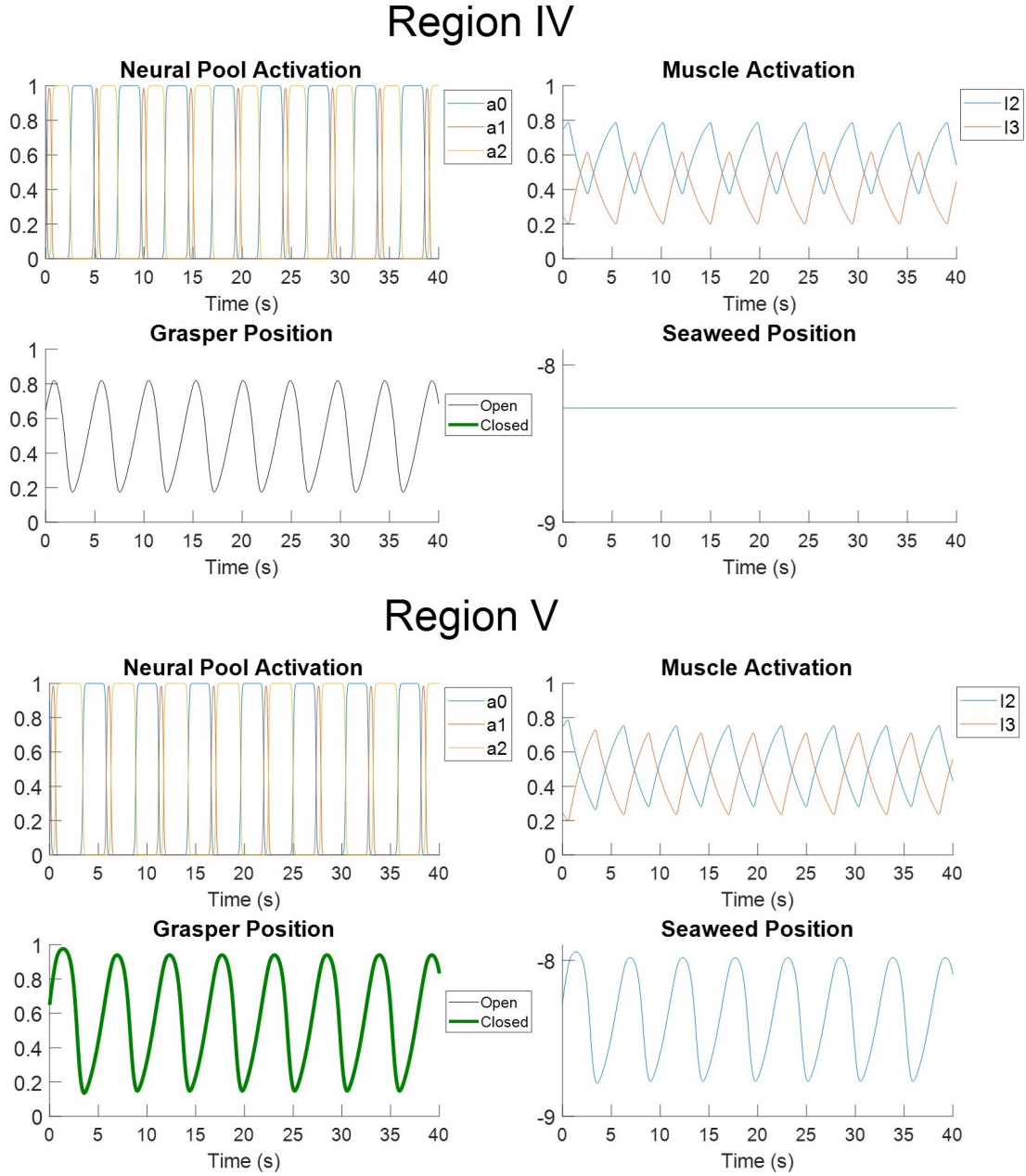


Fig. 16: State variables from the neutral regions **IV-V**. The grasper is always open in region **IV**, so there is no change in seaweed position. In region **V**, the grasper and seaweed have the same rate of change in position because the grasper is always closed.

a_0 , and both the a_0 and a_1 fixed points, respectively. As was the case for the difference in rate of seaweed movement between regions **II** and **III**, we find that region **VII** produces a stronger rejection than region **VI** ($0 > S_{VI} > S_{VII}$) because the a_0 neural pool is active for a

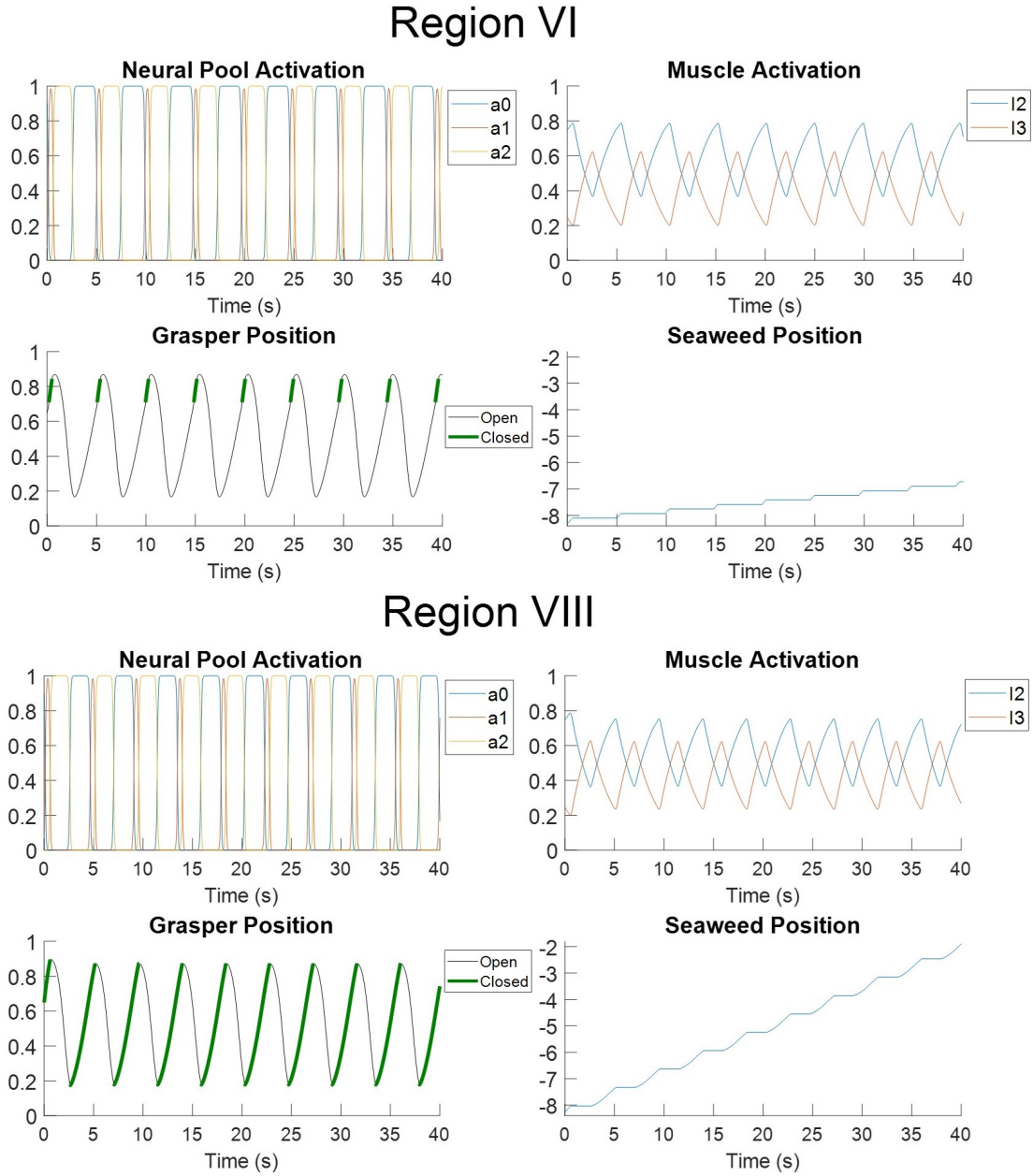


Fig. 17: The state variables from the rejection regions **VI-VIII**. Here, the grasper is only closed when it is protracting. Region **VII** is not shown because it is qualitatively similar to region **VIII**, but with a slightly weaker rejection response ($0 > S_{\text{VII}} > S_{\text{VIII}}$) due to a shorter protraction-closed phase.

longer duration than the a_1 pool (Fig. 17). Similarly, region **VIII** has the greatest rejection rate because the grasper-closed region encompasses both the a_0 and a_1 fixed points, which maximizes the duration of the protraction-closed phase.

Examining Figs. 15, 16 and 17, we observe that the length of time for each period differs between the regions, which affects how the seaweed position changes over time. We define the period of each region to be T_j , where $j \in [\mathbf{I}, \mathbf{II}, \dots, \mathbf{VIII}]$.

In Lytle et al. [13], the authors observed that sensory feedback causes the grasper to pull longer and with more force in the heteroclinic regime than in the limit cycle regime. When confronted with an increased external load, the neural trajectories respond by causing a further increase in both duration and intensity of the retraction-closed phase (the model slug pulls “longer and stronger”), which gives the system additional robustness to this type of perturbation. Here, we observe that among the eight example parameter sets considered, the ingestive regions (**I-III**) have limit cycles with longer net periods than the egestive regions (**VI-VIII**). In particular, the limit cycle period across the different regions from shortest to longest is region **VII**, **VIII**, **IV**, **VI**, **III**, **V**, **I**, and **II**. When the grasper is open, the change in position obeys $\frac{dx_r}{dt} = \frac{F_{\text{musc}}}{b_r}$, so the rate of change is dependent only on the muscle dynamics. The grasper-open dynamics is captured in region **IV**. When the grasper is closed, $\frac{dx_r}{dt} = \frac{F_{\text{musc}} + F_{\text{sw}}}{b_r + b_{\text{sw}}}$. During the protraction-closed phase, the muscle and the seaweed are exerting force in the same direction which allows for a higher rate of change in position and a shorter period. In contrast, swallowing regions have the longest periods, because F_{musc} and F_{sw} act in opposite directions.

Another way to think about the frequency is to consider when the trajectory is in the open versus the closed domains. When the grasper is closed during a_2 activation, this will generate stronger ingestion force in opposition to the seaweed force. When the grasper is closed during a_0 activation, the grasper and seaweed move together quickly because the two forces reinforce each other.

In summary, limit cycle trajectories with (δ, θ) values from a given parameter region exhibit similar qualitative behavior, due to the grasper-closed regions encompassing the same fixed points (Fig. 11). Thus, the parameter regions allow us to predict the qualitative behavior of trajectories of the state variables and approximately predict the quantitative value of seaweed movement rate S . By changing the parameterization of the closing condition, we produced a wide range of biologically plausible grasper behaviors, including swallowing (**I-III**), grasper always open (non-closing) (**IV**), uninterrupted engagement (constantly closed) (**V**), and rejection (**VI-VIII**). We consider the biological relevance of each of these behaviors further in the Discussion section.

4 The Effect of Load on Fitness

For the sake of survival, robust rhythmic motor systems must maintain their performance despite constantly changing environmental conditions. Consider walking, a sequence of rhythmic limb movements. We never walk in “ideal” settings without any impedance; instead, we regularly encounter a number of small obstacles: there may be a small bump in the road, the wind may be pushing against us, or there may be an obstacle in our path. Our body and brain work together to adjust to these environmental changes through sensory feedback, to allow us to continue walking.

Similarly, the sea slug’s feeding pattern generator adapts its behavior to accommodate impediments to ingestion. The papers introducing the Shaw/Lyttle model [13, 22] address how the slug’s grasper responds to one such challenge: changes in the force with which seaweed resists ingestion. In the heteroclinic regime ($\mu \lesssim 1.7 \times 10^{-5}$) sensory feedback allows the model to respond to increasing seaweed forces by extending the duration of retraction. In the previous chapter, we modified the closing condition and identified eight parameter regions each producing distinct grasper behaviors. In Section 4.1, we will examine robustness of each parameter regime across different seaweed forces.

However robust, a motor system cannot maintain its performance when the countervailing external forces are too strong. Referring to the earlier example, there are circumstances when we can no longer walk: the wind may be blowing too strongly against us, or the hill may become too steep. In Section 4.2, we investigate what happens when the seaweed force overpowers the grasper.

4.1 Varying Seaweed Force across Parameter Regions

We vary the seaweed force $F_{\text{sw}} \in [-0.1, 0.15]$ for each of the eight parameter regions and evaluate changes in S , the average rate of seaweed movement. Although negative seaweed forces would not occur naturally in normal, pliant seaweed, they could occur transiently if tidal surge pressed a sea slug towards a particularly stiff stalk of seaweed which it was swallowing. In general, given the mathematical model in which F_{sw} appears as a parameter, we can ask for the model's behavior for a range of both positive and negative values of F_{sw} separately from any physical interpretation.

When the load resisting ingestion becomes too great ($F_{\text{sw}} > 0$ becomes large), the grasper behavior may no longer be periodic (for further discussion, see Section 4.2). Therefore, we define the average rate of seaweed movement to be $S \equiv 0$ when there does not exist a stable periodic orbit. Fig. 18 shows the rate of seaweed movement (positive S reflects inward movement, or ingestion; negative S reflects outward movement, or egestion) as a function of F_{sw} for a representative system from each of parameter region I-VIII.

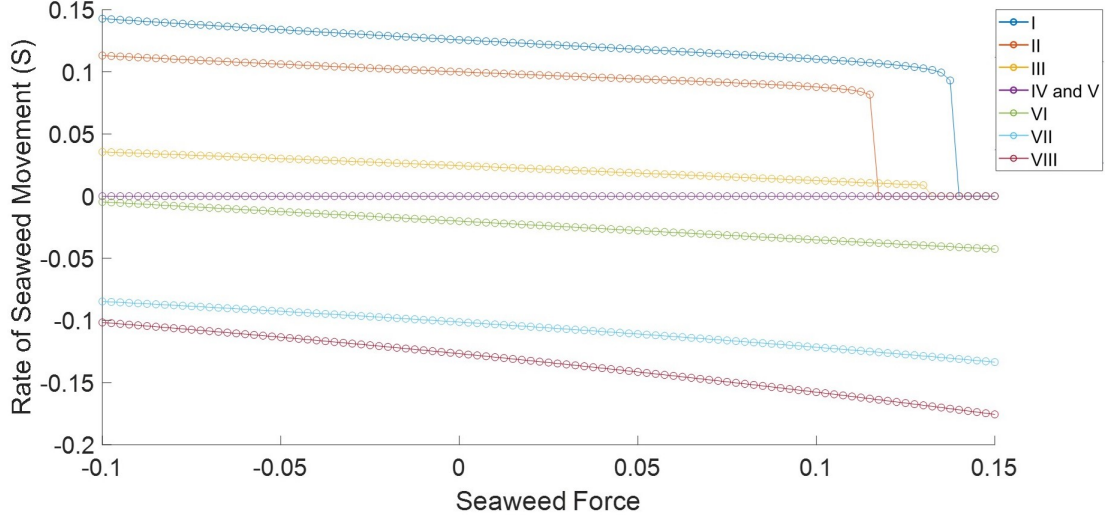


Fig. 18: Rate of seaweed movement for each parameter region at varying levels of seaweed force. A representative set of parameters was drawn from each of the eight parameter regions (see Fig. 14). In each region S decreases as a function of F_{sw} , except in regions **IV** and **V** in which it remains constant at $S = 0$. When the grasper in regions **I**, **II**, **III**, and **V** encounter large forces that cause the periodic motion of the grasper to collapse, the rate is defined to be $S \equiv 0$.

Recall that the parameter regions were defined with $F_{sw} = 0.1$ such that $S_{\mathbf{I}} \geq S_{\mathbf{II}} \geq \dots \geq S_{\mathbf{VIII}}$ (Section 3.1). As Fig. 18 shows, the inequality remains consistent across all values of the seaweed force as long as the net seaweed movement is nonzero for all non-neutral regions.

In the ingestion regions **I-III**, the grasper maintains its ingestive behavior until F_{sw} becomes too great and causes a sudden drop in the rate of seaweed movement from $S > 0$ to $S = 0$.

In regions **I**, **II**, and **III**, the periodic limit cycle movement of the grasper loses stability at $F_{sw} \geq 0.1376$, $F_{sw} \geq 0.1162$, and $F_{sw} \geq 0.131$, respectively. In the neutral regions, the grasper movement induces no net seaweed movement ($S = 0$) regardless of F_{sw} . In

region **IV**, the grasper never contacts the seaweed, so the seaweed position is fixed (Section 1.1). The grasper in region **V** is always closed, but $S = 0$ for two separate reasons. When

$F_{sw} < 0.1138$, the neuromotor trajectory is a stable limit cycle, and the seaweed oscillates with that of the grasper with no net change in position. In contrast, if $F_{sw} \geq 0.1138$, the

periodic behavior of the grasper collapses due to the strong seaweed force, much like the case in the intake regions. In comparison with the previous parameter regions, the grasper in the rejection regions (**VI-VIII**) always maintains its stable oscillation and ejects seaweed ($S < 0$), regardless of the seaweed force. The analysis of parameter regions from the previous chapter appears consistent despite varying the seaweed force, even when the force is negative.

Fig. 18 shows the average rate of seaweed movement measured as the net change in position divided by the net change in time. Consistent with previous observations [13, 22], the decline of S as a function of increasing F_{sw} is remarkably gradual, a sign that the system is robust to externally applied loads [13]. In order to understand this robustness in more detail, we analyze the change in seaweed position per period along with the change in period, as F_{sw} increases. In Fig. 19 we plot the net change in position against the oscillation period.

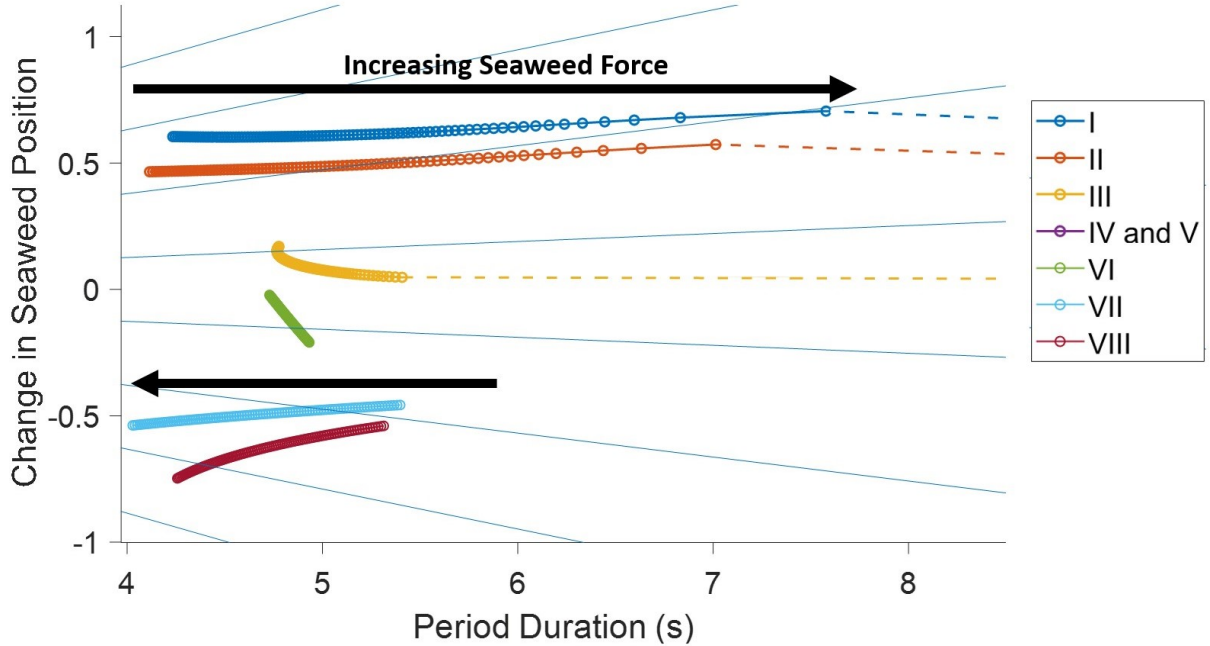


Fig. 19: Change in seaweed position and period for different seaweed force $F_{sw} \in [-0.1, 0.15]$. Each point represents a point from Fig. 18. The points with no change in seaweed position are discarded and are shown as dashed lines connecting to $(t, x_{sw}) = (30, 0)$. Thin blue lines are level curves of the fitness function $S = \Delta x/T$. These level curves are constant rates of seaweed movement with positive and negative slopes corresponding to ingestion and egestion, respectively. As the arrow indicates (black), in regions **I**, **II**, **III**, and **VI**, the seaweed force increases from left to right while the force increases in the opposite direction for regions **VII** and **VIII**.

Points where $S = 0$ are not shown, i.e. regions **IV** and **V** and the values where the load overwhelms the periodic behavior of the grasper. The blue lines in the figure are level curves representing constant rates of seaweed movement. Therefore, the fewer level curves crossed as the force increases, the smaller the decrease in fitness. The slopes of the lines from regions **I** and **II** remain slightly above zero in the figure which represents a slow decrease in ingestion, with **I** decreasing slightly faster. In both of these regions, the amount of seaweed ingested per period does not decrease but increases slightly; however, the decrease in the rate of seaweed movement is due to the increasing time needed for each period. This behavior confirms the earlier observation [13, 22] that robustness is achieved by the neuro-motor system pulling

“longer and stronger” on each power stroke of the ingestive movement, in regions **I-II**. Unlike the two other intake regions, region **III** is much less resilient to changes in seaweed force, and the amount of seaweed ingested per period drops rapidly. As anticipated, regions of higher intake (**I** and **II**) are more resilient and counteract the increase in load by increasing the time per period.

From the rejection regions, region **VI** behaves qualitatively similarly to the previous regions, but regions **VII** and **VIII** exhibit distinct position to duration ratios. In region **VI**, any increase in load results in more seaweed loss and longer periods. Note that the rate of seaweed movement will never become positive in this region, and more negative seaweed forces would result in reduced seaweed rejection ($S \rightarrow 0$). In regions **VII** and **VIII**, the period duration decreases with increasing seaweed force while more seaweed is rejected per period. Because the seaweed and the grasper move together, the increasing seaweed force is pulling in the direction of protraction, which facilitates rejection and causes the rapid change in the grasper position. Therefore, the length of time per period is decreased, resulting in a grasper behavior unlike any of those observed in the previous regions.

4.2 Collapse of the Feeding Rhythm

Like any biomechanical system, rhythmic movements of *Aplysia californica*’s grasper can be arrested by a sufficiently large opposing force. In the previous section, we established that varying the seaweed force parameter (F_{sw}) can produce a collapse of the motor pattern in certain regions (Fig. 18). Specifically, the trajectory ceases to be a limit cycle when $F_{sw} \geq 0.1376, 0.1162, 0.1310,$ and 0.1138 in regions **I, II, III,** and **V**, respectively.

In order to understand the mechanism of collapse, we consider trajectories beginning from a common initial condition with seaweed force just above or just below the collapse point. Let \mathbf{y} represent the combined brain and body dynamics from Eq. (1), that is we set $\mathbf{y} = [\mathbf{a}; \mathbf{x}] \in \mathbb{R}^6$, and we write

$$\frac{d\mathbf{y}}{dt} = \mathbf{p}(\mathbf{y}, F_{\text{sw}}) = \begin{pmatrix} \mathbf{f}(\mathbf{y}) + \epsilon \mathbf{g}(\mathbf{y}) \\ \mathbf{h}(\mathbf{y}) \end{pmatrix} + F_{\text{sw}} [[\text{grasper closed}]] \begin{pmatrix} 0 \\ 0 \\ 0 \\ 0 \\ 0 \\ 1 \end{pmatrix} \quad (22)$$

Here, $[[\text{grasper closed}]]$ is the indicator function that is 1 when the grasper is closed and 0 otherwise. Note that we do not consider the seaweed position in \mathbf{y} because we can evaluate the seaweed position using the grasper position.

Let \mathbf{y}_1 and \mathbf{y}_2 be the trajectories when $F_{\text{sw}} = 0.1161$ and $F_{\text{sw}} = 0.1162$, respectively (cf. Fig. 20). The common initial condition begins when the grasper is in the protraction-open phase (Table 1). The rates of change $\frac{d\mathbf{y}_1}{dt} = \mathbf{p}_1(\mathbf{y}_1)$ and $\frac{d\mathbf{y}_2}{dt} = \mathbf{p}_2(\mathbf{y}_2)$ differ such that

$$\mathbf{p}_2(\mathbf{y}) = \mathbf{p}_1(\mathbf{y}) + \eta \mathbf{q}(\mathbf{y}). \quad (23)$$

We set $\eta \mathbf{q}(\mathbf{y})$ to be the difference term with magnitude η which represents the size the change in seaweed force and is assumed to be small.

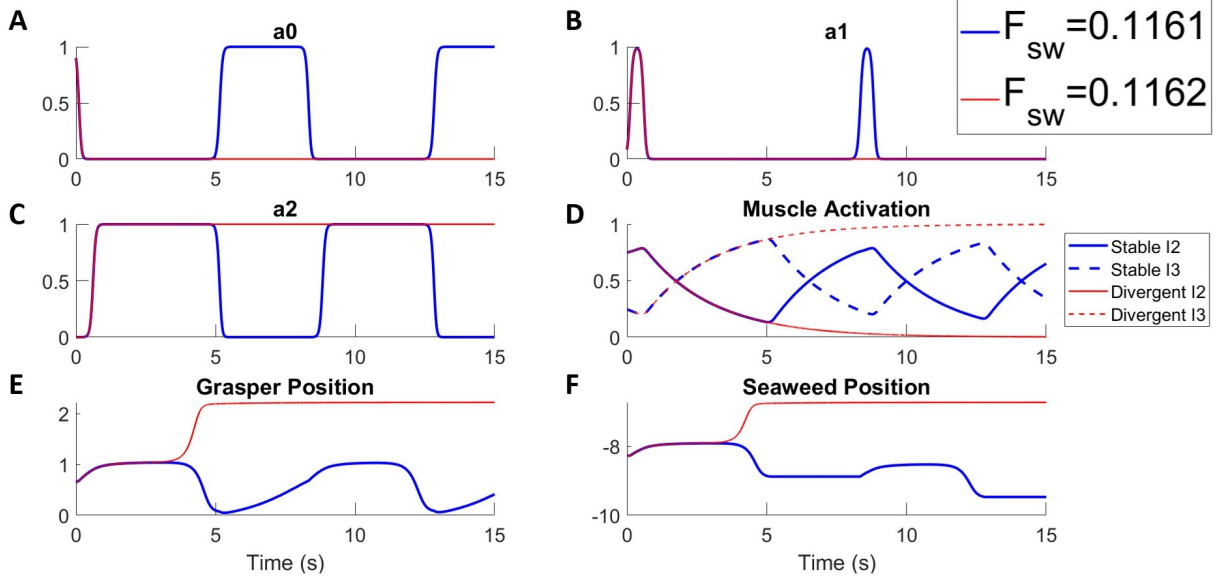


Fig. 20: Collapse of grasper movement intake region **II**. The grasper behavior is periodic (blue) when the seaweed force is not overpowering. The a_0 (**A**) and a_1 (**B**) neural pools can no longer oscillate and remain fully inactivated when the seaweed force is too great (red). In contrast, the a_2 pool is fully activated to counteract the seaweed force. As a result of differences in the neural dynamics, the muscle activities (**D**) of I2 (solid) and I3 (dashed) undergo a qualitative change, as well. The grasper (**E**), unable to retract, is pulled by the seaweed force past its maximum protraction position of 1. (**F**) Changes in the seaweed position correspond to changes in the grasper position.

As Fig. 20 shows, the variables of the two trajectories behave differently; however, we cannot easily discern which variable diverges first using this figure. Therefore, we investigate $\mathbf{z}(t)$, the differences between the trajectories:

$$\mathbf{z}(t) = \mathbf{y}_2(t) - \mathbf{y}_1(t). \quad (24)$$

At the initial value, the grasper is open and $\mathbf{z}(0) = \mathbf{0}$. The grasper remains open until $t_0 = 0.116$, after which the grasper closes and the trajectories begin to diverge. Thus we consider the evolution of \mathbf{z} starting from initial condition $\mathbf{z}(t_0) = \mathbf{0}$. Initially both \mathbf{z} and η are small. Numerically, we observe that $|\mathbf{z}|$ and η remain the same order, at least initially. To understand how the grasper oscillation collapses, we develop a Taylor expansion in both

η and $|\mathbf{z}|$.

$$\begin{aligned}
\frac{d\mathbf{z}}{dt} &= \mathbf{p}_2(\mathbf{y}_2) - \mathbf{p}_1(\mathbf{y}_1) \\
&= \mathbf{p}_2(\mathbf{y}_1 + \mathbf{z}) - \mathbf{p}_1(\mathbf{y}_1) \\
&= \mathbf{p}_1(\mathbf{y}_1 + \mathbf{z}) + \eta \mathbf{q}(\mathbf{y}_1 + \mathbf{z}) - \mathbf{p}_1(\mathbf{y}_1) \\
&= \mathbf{p}_1(\mathbf{y}_1) + D\mathbf{p}_1(\mathbf{y}_1) \cdot \mathbf{z} - \mathbf{p}_1(\mathbf{y}_1) + \mathcal{O}(|\mathbf{z}|^2) + \eta \mathbf{q}(\mathbf{y}_1 + \mathbf{z}) \\
&= D\mathbf{p}_1(\mathbf{y}_1) \cdot \mathbf{z} + \mathcal{O}(|\mathbf{z}|^2) + \eta \mathbf{q}(\mathbf{y}_1 + \mathbf{z}) \\
&= D\mathbf{p}_1(\mathbf{y}_1) \cdot \mathbf{z} + \mathcal{O}(|\mathbf{z}|^2) + \eta \mathbf{q}(\mathbf{y}_1) + \eta D\mathbf{q}(\mathbf{y}_1) \cdot \mathbf{z} + \mathcal{O}(\eta^2).
\end{aligned}$$

Here, D is the derivative, $D\mathbf{p}$ is the 6×6 Jacobian matrix (calculated when the grasper is closed), and $|\mathbf{z}|$ is the Euclidean norm of \mathbf{z} .

The seaweed force is the only term that causes \mathbf{p}_1 and \mathbf{p}_2 to differ, so $\eta \mathbf{q}(\mathbf{y}_1) = 0.1162 - 0.1161 = 10^{-4} \hat{\mathbf{e}}_6$, where $\hat{\mathbf{e}}_6$ is a unit vector along the grasper axis (cf. Eq. (22)). Therefore, as long as $|\mathbf{z}| \leq \mathcal{O}(\eta)$,

$$\frac{d\mathbf{z}}{dt} = D\mathbf{p}_1(\mathbf{y}_1) \cdot \mathbf{z} + \eta \mathbf{q}(\mathbf{y}_1) + \mathcal{O}(\eta^2) = D\mathbf{p}_1(\mathbf{y}_1) \cdot \mathbf{z} + 10^{-4} \hat{\mathbf{e}}_6 + \mathcal{O}(\eta^2). \quad (25)$$

The initial divergence of trajectories is captured by the linear inhomogeneous approximation

$$\frac{d\mathbf{z}}{dt} = D\mathbf{p}_1(\mathbf{y}_1) \cdot \mathbf{z} + 10^{-4} \hat{\mathbf{e}}_6. \quad (26)$$

We evaluate the Jacobian of the model equations $D\mathbf{p}$ as follows:

$$D\mathbf{p} = \begin{pmatrix} \frac{1-a_0-\gamma a_1}{\tau_a} & -\frac{\gamma a_0}{\tau_a} & 0 & 0 & 0 & -\epsilon \\ 0 & \frac{1-a_1-\gamma a_2}{\tau_a} & -\frac{\gamma a_1}{\tau_a} & 0 & 0 & \epsilon \\ -\frac{\gamma a_2}{\tau_a} & 0 & \frac{1-a_2-\gamma a_0}{\tau_a} & 0 & 0 & \epsilon \\ \frac{u_{\max}}{\tau_m} & \frac{u_{\max}}{\tau_m} & 0 & -\frac{1}{\tau_m} & 0 & 0 \\ 0 & 0 & \frac{u_{\max}}{\tau_m} & 0 & -\frac{1}{\tau_m} & 0 \\ 0 & 0 & 0 & -\phi\left(\frac{x_r-c_0}{w_0}\right) & \phi\left(\frac{x_r-c_1}{w_1}\right) & \frac{\delta}{\delta x_r} \frac{F_{\text{musc}}+F_{\text{sw}}}{b_r+b_{\text{sw}}} \end{pmatrix},$$

$$\begin{aligned} \frac{\delta}{\delta x_r} \frac{F_{\text{musc}} + F_{\text{sw}}}{b_r + b_{\text{sw}}} &= \frac{\kappa u_0}{w_0(b_r + b_{\text{sw}})} \left[\left(\frac{x_r - c_0}{w_0} - 1 \right) \left(\frac{x_r - c_0}{w_0} + 1 \right) \right. \\ &\quad \left. + \frac{x_r - c_0}{w_0} \left(\frac{x_r - c_0}{w_0} + 1 \right) + \frac{x_r - c_0}{w_0} \left(\frac{x_r - c_0}{w_0} - 1 \right) \right] \\ &\quad - \frac{\kappa u_1}{w_1(b_r + b_{\text{sw}})} \left[\left(\frac{x_r - c_1}{w_1} - 1 \right) \left(\frac{x_r - c_1}{w_1} + 1 \right) \right. \\ &\quad \left. + \frac{x_r - c_1}{w_1} \left(\frac{x_r - c_1}{w_1} + 1 \right) + \frac{x_r - c_1}{w_1} \left(\frac{x_r - c_1}{w_1} - 1 \right) \right]. \end{aligned}$$

Note that when the grasper is open, the model equations obeys a different system of ODEs (Section 1.1). Moreover, when the trajectory crosses from the open to the closed region (or vice-versa) there is a discontinuous jump in the vector field. For these reasons, the Jacobian $D\mathbf{p}$ is not well defined at the opening/closing boundary, and additional factors must be considered when evaluating the linear response to perturbations. These considerations go beyond the scope of this thesis but are considered in [25].

Evaluating $\frac{dz}{dt}$ reveals that divergence in the grasper position is the event that leads to the collapse of the grasper oscillation. In Fig. 21, we plot $\frac{dz}{dt}$ and compare the rate of change in the difference between the state variables of the stable and divergent trajectories.

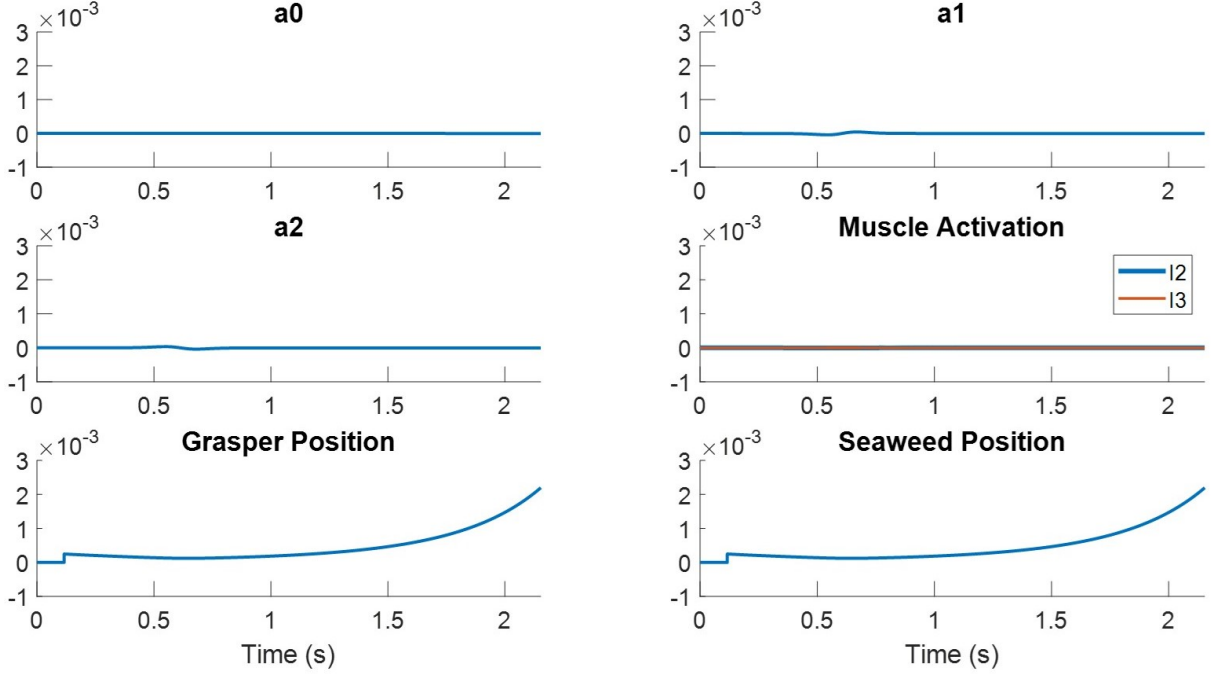


Fig. 21: Rate of change in the difference between state variables ($\frac{dz}{dt}$) from the trajectories (Fig. 20) in region **II**. Initially, there are no differences between the two trajectories because the grasper is still open ($0.116 \leq t$). The rate change of the difference in the grasper position deviates from zero upon closing, while the other state variables remain approximately constant. The rate of change in the difference in seaweed positions equals that of the grasper, for the time interval shown. In order to focus on the initial small deviation due to changing the force, the graphs terminate when $10^{-3} \leq |\mathbf{z}|$.

The rate of change of the differences in grasper position (Fig. 21 (E)) increases faster than the rates of change of the other state variables. Until around $t = 2$, $z_i \approx 0$ for all components of \mathbf{z} , except for the 6th (grasper) component. Consequently, we can approximate the rates of change of differences to be:

$$\frac{d\mathbf{z}}{dt} \approx D\mathbf{p}_1(y_1) \cdot \mathbf{z} + 10^{-4} \hat{\mathbf{e}}_6 = \mathbf{z}_6 \begin{pmatrix} -\epsilon \\ \epsilon \\ \epsilon \\ 0 \\ 0 \\ \frac{\delta}{\delta x_r} \frac{F_{\text{musc}} + F_{\text{sw}}}{b_r + b_{\text{sw}}} \end{pmatrix} + 10^{-4} \hat{\mathbf{e}}_6. \quad (27)$$

For Figs. 20-21, $\eta = 10^{-4}$. Because $\epsilon = 10^{-4}$ (Table 2 of Appendix A.1) and $|\mathbf{z}| \leq 10^{-3}$, the

neural components of Eq. (27) remain small relative to $\eta \mathbf{q} = 10^{-4} \hat{\mathbf{e}}_6$. As a result, not much change in the rate of change in the difference is observed in any variable besides the grasper for the first two seconds of the simulation in Fig. 21. However, the divergence between the grasper position of the two trajectories eventually causes the trajectories to deviate from one another.

The timing of the grasper closing explains why certain parameter regions can resist a wider range of seaweed forces. The grasper is only affected by the seaweed force when the grasper is closed (Section 1.1). In order to generate the strongest muscle force possible, the grasper cannot be too far protracted or retracted when the a_2 neural pool, responsible for activating the I3 retractor muscle, is fully activated (Fig. 22).

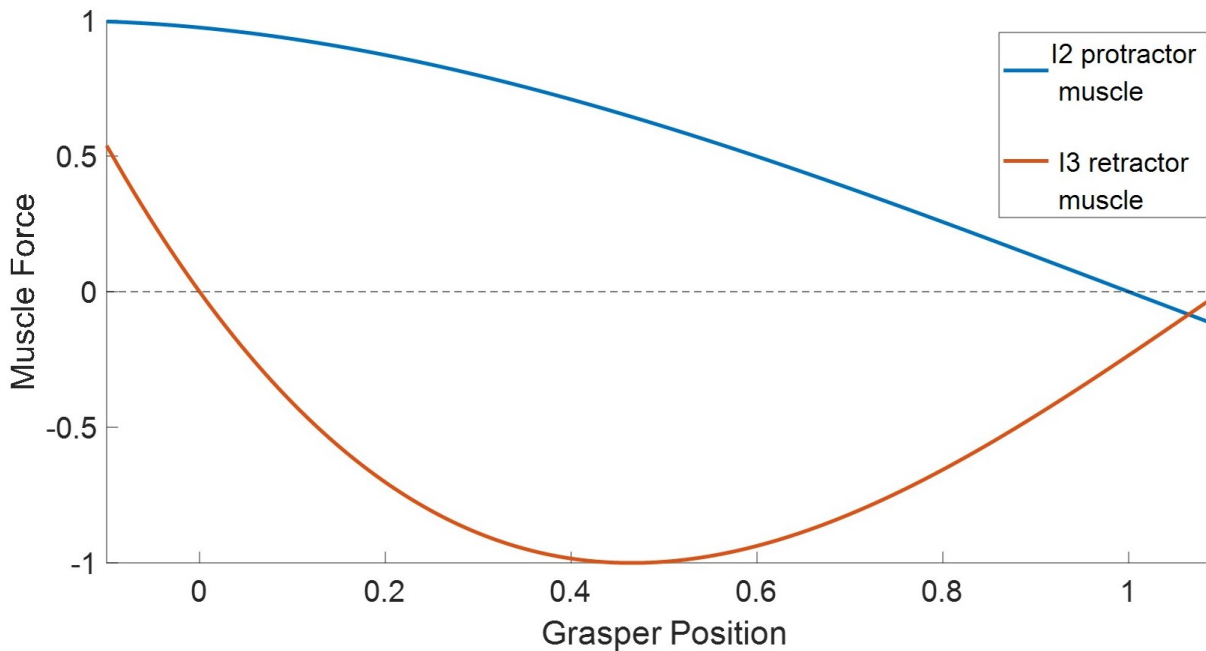


Fig. 22: Length-tension curve of the I2 and I3 muscles. Normally, the grasper range is between 0 (maximum retraction) and 1 (maximum protraction). Negative and positive forces contribute to protraction and retraction, respectively. The model I3 muscle produces almost no force near maximum protraction or retraction. The I2 muscle generates more force as the grasper retracts and produces no force when the grasper is fully protracted. The force generated by each muscle is scaled by the I2 and I3 muscle activation variables u_0 and u_1 , respectively, both of which range from 0 to 1.

In region **II**, $F_{\text{sw}} = 0.1162$ is just strong enough to pull the grasper out such that it cannot generate sufficient force to counteract the seaweed force. For the same force value, the grasper in regions **I** and **III** is able to resist the seaweed force and successfully perform ingestion because the model slug has maximized the time spent closed when a_2 is strongly activated, and remains open during other times (Fig. 23). In particular, the grasper in region **I** is only closed when the neural trajectory is near high a_2 activation, which allows the muscles to generate large retraction forces. Despite having a weaker ingestion than region **II** for $F_{\text{sw}} \leq 0.1161$, region **III** is capable of handling a wider range of seaweed forces. Region **V** can operate in the smallest range of the seaweed force. In this neutral region, the grasper is always closed, which maximizes the grasper protraction-closed phase, so the grasper has already protracted too far by the time I3 is innervated to generate enough muscle force against the seaweed to continue the oscillation.

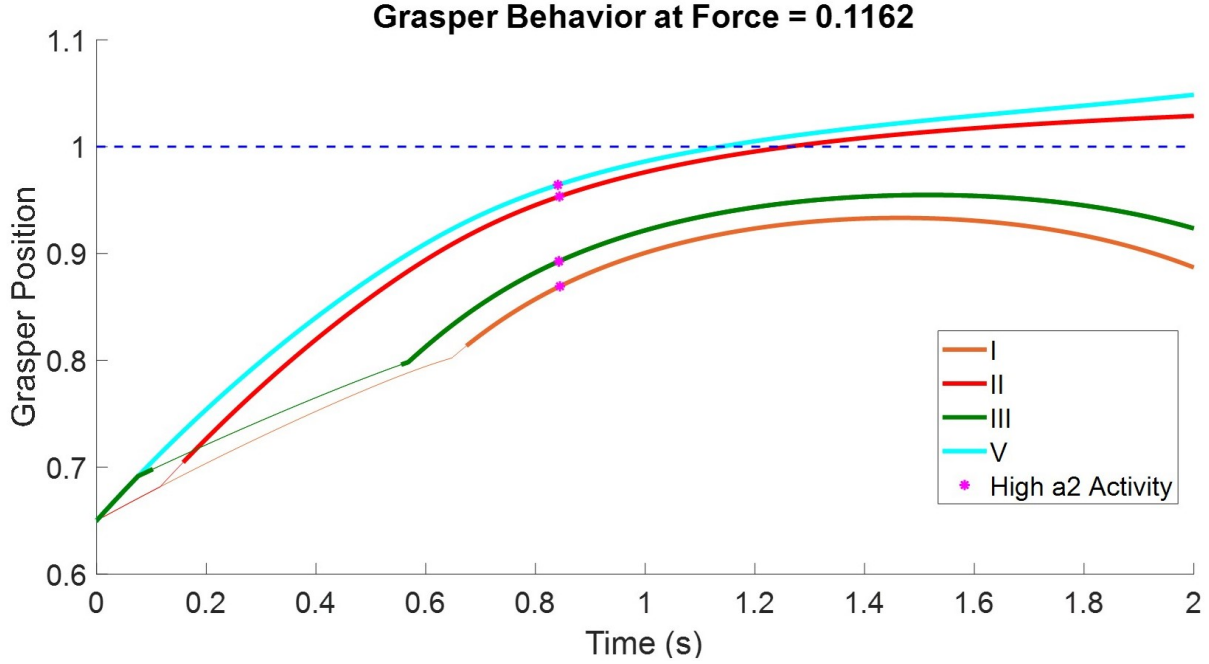


Fig. 23: Grasper behaviors in parameter regions **I**, **II**, **III**, and **V** at $F_{sw} = 0.1162$. When the grasper is closed (bold), the sum of the muscle and seaweed forces controls the rate of change of the grasper position. For ingestion, the grasper would, ideally, be closed only near the high activity of the a_2 neural pool (magenta), or when $0.99 \leq a_2$. However, in regions **II** and **V**, the grasper is almost fully protracted (dashed blue line) when a_2 is fully activated, so the I3 muscle cannot generate enough retraction force to oppose the seaweed force. In contrast, the grasper in regions **I** and **III** was able to counteract the seaweed force because the grasper generally closed only when there was strong a_2 activity.

The collapse in feeding rhythm is not observed in all regions for strong seaweed forces ($0.1138 \lesssim F_{sw}$). In the rejection regions (**VI-VIII**), the grasper can maintain oscillation because the muscle and the seaweed force are acting in the same direction when the grasper is closed. The grasper in region **IV** is always open, so its periodic trajectory is unaffected by the seaweed force.

5 Discussion

5.1 Interpreting the Parameter Regions

In this thesis, we parameterized the closing condition (Eq. (16)) of the *Aplysia californica* grasper model [13, 22] and systematically varied (δ, θ) to test the sensitivity of these parameters. We grouped combinations of parameters into eight distinct parameter regions (Chapter 3) based on the rate of seaweed movement (S) such that $S_{\mathbf{I}} \geq S_{\mathbf{II}} \geq \dots \geq S_{\mathbf{VIII}}$. The original closing condition (Eq. (9)) belongs to region **II**. These regions, each with their own distinct grasper behavior, can be further classified into one of the three types: intake, neutral, or rejection regions.

We could interpret the different parameterizations, which are subtle differences in how the grasper closing condition is defined, as neuromodulation. Neuromodulation can alter firing properties of neurons or induce changes in synaptic strengths, which is different from neurotransmission’s effect of exciting or inhibiting neurons. Some of the effects from neuromodulators are shown in the following examples. In *Aplysia californica*, modulation from serotonin and the egg-laying hormone on the R15 neuron increases the cyclic AMP concentration and induces changes in the underlying calcium and potassium currents, which causes the R15 neuron to have more spikes per burst while increasing the amplitude of hyperpolarization between firing [11]. When dopamine act as a neuromodulator, certain synapses in the crustacean stomatogastric system are strengthened while others are weakened which serves as a system of “checks and balances” used to regulate the pyloric network [3]. Not only do these modulators introduce flexibility in function to a motor pattern generator but they are also essential to maintaining rhythmic movements. For example, neuromodulation

from serotonergic neurons is intrinsic to the Tritonia swim pattern circuit and necessary for swimming to occur [8]. Another example is in the regulation of the accessory radula closer muscle in *Aplysia californica*. The B15 and B16 neurons release acetylcholine and co-transmitters to regulate contraction and relaxation in this muscle [8].

Referring back to the original parametrization of the opening/closing threshold (Eq. (11)) neuromodulation could affect the synaptic weights (represented by γ and β) or change the threshold for activation of a muscle closing the grasper (δ). Although actively changing the open/close boundary is beyond the scope of our analysis here, we can imagine situations in which the sea slug uses neuromodulation to adapt its strategy to different circumstances.

Manipulating neuromodulation in the laboratory would require specific chemicals, which can make the process difficult and expensive. By experimenting with the parameters of the Shaw/Lyttle model, we can simulate how neuromodulation's effect on the timing of the closing of the grasper can produce distinct grasper behaviors.

The grasper in intake regions **I**, **II**, and **III** ($S > 0$) undergoes protraction-open, protraction-closed, and retraction-closed phases of motion to generate swallowing. The grasper in neutral region **IV** ($S = 0$) always remains open, so the seaweed position does not change. We characterize this behavior as grasper always open (non-closing). In theory, it may be possible to innervate the grasper in such a way that the grasper never closes even as it protracts and retracts, but this behavior has not been observed *in vivo*.² However, a situation could arise in which the slug bites a large object that becomes stuck, so the slug does not need to exert any force to hold the object in place while the grasper moves. In neutral region **V**, the grasper undergoes lockdown (always closed) so the seaweed and grasper oscillates together which

²Dr. J.P. Gill, personal communication.

results in net zero intake. This behavior has been referred to as the “intermediate pattern” by Morton and Chiel [16] which occurs when the slug feeding behavior is transitioning from ingestion to egestion. The authors suggested that the slug may be attempting to “reposition partially swallowed food” or to induce mechanical fatigue to tear the object in its grasper. The closing condition from the rejection regions **VI**, **VII**, and **VIII** ($S < 0$) cause the grasper to be closed during protraction and open during retraction which simulates the slug rejecting seaweed.

The eight parameter regions correspond to unique strategies available to *Aplysia californica*. When $F_{sw} \in [-0.1, 0.1137]$, which is a range where the grasper behavior is periodic (Section 4.1) regardless of the parameterization, the stronger of the intake and rejection regions have unique strategies in response to an increasing seaweed force. Despite the increasing load, regions **I-II** increase the duration of the retraction-closed phase to bring in more seaweed at the cost of longer periods. In contrast, the rejection regions **VII-VIII** responds to large seaweed forces by decreasing the period for each rejection cycle which increases the rate of egestion.

Different grasper behaviors are more suitable for handling different levels of seaweed force. For example, suppose a force transducer [23] is pulling on a tough object, such as nori seaweed layered around a strip of tough, double-sided tape, with a force greater than what the grasper can generate. If the slug grasper is undergoing lockdown (region **V**), then the grasper will eventually be pulled out of the slug’s mouth. A more appropriate response from the animal could be to eject (regions **VI-VIII**) the taped seaweed. Suppose instead that the seaweed force is slightly weaker so some intake regions can still bring in seaweed. Regions **I** and **III** can handle stronger forces than region **II**. As we analyzed in Section 4.2,

the timing of the grasper closing is crucial in determining how much force the grasper can exert on the seaweed. To combat a powerful load, the grasper cannot be near full protraction during strong a_2 activity; or else, the I3 muscle cannot generate near the full potential of its retractive force. Even though region **II** brings in more seaweed when $F_{sw} \leq 0.1161$, the grasper in this regions can handle a smaller range of force than in region **III**, which represents slow but strong ingestion. Region **I** is the strongest mode of ingestion, which may cost more energy than the other regions; therefore, if the slug is not in urgent need of food, it could instead deploy regions **II** or **III**, thus making region **III** even more appealing if the seaweed is offering strong resistance.

In Chapter 4, we experimented with different grasper behaviors confronted with both positive and negative seaweed forces. As explained previously, one way to interpret negative seaweed forces is to consider if tidal surge were to push the animal against a stiff stalk of seaweed. Alternatively, if the slug has gripped a stiff object, such as a polyethylene tube, then a force could be applied to push the object towards the slug. Previous experiments have been performed using polyethylene tubes to elicit rejection behaviors from *Aplysia californica* [17, 16]. While experimenters did not push the tube past the grasper and further into the animal, such a task could be possible either *in vivo* or for an isolated buccal mass [15].

While certain behaviors are more appropriate in response to different loads, some parameter regions are more advantageous because they can more readily transition to other regions and behaviors. Each of the regions corresponds to either including or excluding each of the three fixed points from the closed region. Therefore, the eight regions may be identified with the corners of the cube $\{0, 1\}^3$ (Fig. 24). Let us consider $\sqrt{\Delta\delta^2 + \Delta\theta^2}$ to be the difference in neuromodulation between two parameterizations of the grasper closing condition. The

“easiest” transition between regions will occur between adjacent regions where shifting only δ or θ is necessary to enter a neighboring region.

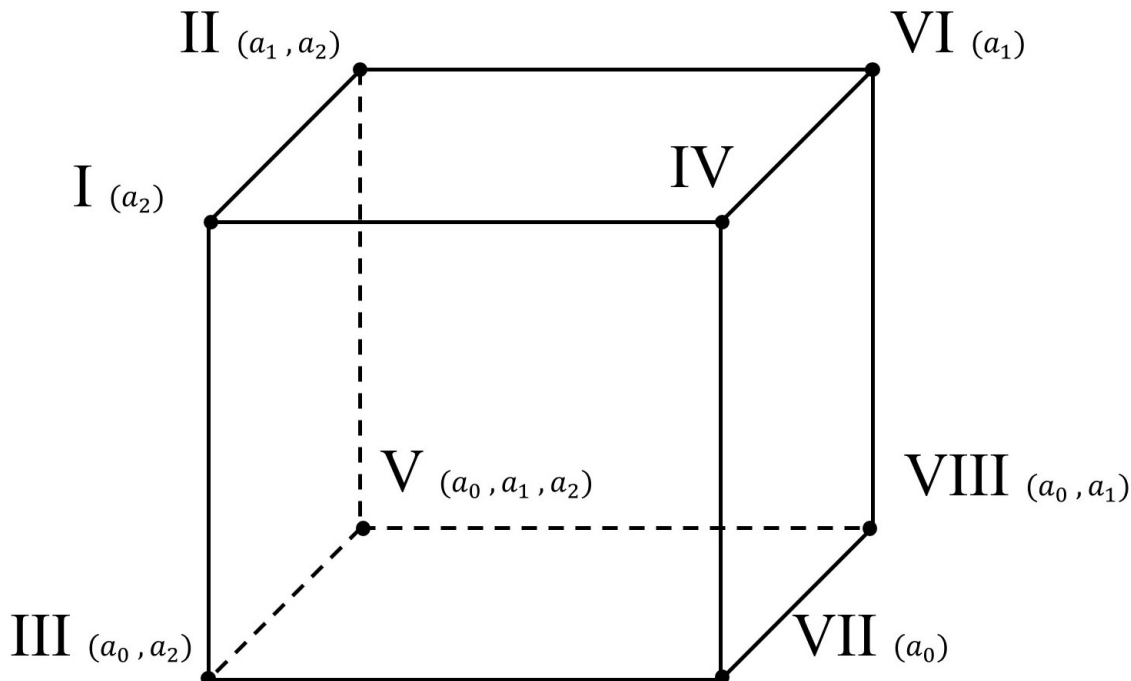


Fig. 24: Adjacent parameter regions. The parameter regions (Fig. 9) are represented as nodes with the edges connecting regions that are separated by a boundary. Each region includes or excludes each of the 3 neural fixed points, forming the cubic structure $\{0, 1\}^3$. The fixed points captured by the grasper-closed space are listed next to each region. Note the “best” and “worst” regions (**I** and **VIII**, resp.) occupy diametrically opposite corners; similarly the 2nd best and 2nd worst (**II** and **VII**, resp.), *et cetera*.

Out of all intake regions, region **I** has the highest rate of ingestion but also the least diverse neighbors. The regions adjacent to region **I** are the other two regions with positive intake (**II** and **III**) and the grasper always open region (**IV**). In contrast, region **II** is connected to regions with rejection (**VI**) and lockdown (**V**) behaviors, and region **III** has similarly diverse neighbors. Suppose that adjacency means less time or energy needs to go into a system to transition to a different region. Then region **II** and **III** would be able to transition to other behaviors more quickly than region **I**. Furthermore, region **II** can retain a much higher rate of intake than region **III**, while also remaining flexible. Therefore, the optimal strategy for

an animal's survival might not be to always remain in regions with the highest intake but in regions that have relatively high intake but can easily transition to other behaviors, thus being more adaptable to different circumstances. Similar conclusions could be drawn about the rejection regions. Although region **VIII** has the highest rate of egestion, the other two regions (**VI** and **VII**) have neighbors with more diverse behaviors.

5.2 Model Limitations

We made some simplifications and followed the assumptions made by [13, 22] to study the underlying mechanisms involved in rhythmic motion. Although we have generalized the neurons controlling the buccal mass into three neural pools and three muscle groups, *Aplysia californica*'s buccal ganglion [12] contains other neurons responsible for stimulating a number of muscles (Fig. 1, Chapter 1) that controls the radula/odontophore [9].

The authors of the Shaw/Lyttle model only considered using the length tension curve $\phi(x_r)$ when $x_r \in [0, 1]$, and the oscillating grasper position was constrained accordingly. In this thesis, we experimented with the seaweed force necessary to produce a collapse in grasper motion in the different parameter regions. For strong enough seaweed forces, the model grasper extended beyond the maximum protraction position ($1 < x_r$). Biologically, this overextension would result in eversion, a fatal condition in which the grasper is pulled out of the mouth. A boundary condition was not imposed on the grasper in our Matlab model because Dr. Wang had developed the code to analyze a different problem: the behavior of limit cycle trajectories with hard boundary conditions imposed on the neural pools [25]. Furthermore, the seaweed forces applied by Dr. Wang were within the range of forces used

by Shaw et al. [22] and Lyttle et al. [13], so the grasper position did not diverge past 1. The analysis performed in this thesis was not affected even when the grasper diverged, but a future improvement to our implementation of the model could be to impose a hard boundary on the position of the grasper.

In the Shaw/Lyttle model, the seaweed position is assumed to be fixed whenever the grasper is open. After *Aplysia californica*'s grasper (*in vivo*) retracts to swallow seaweed, the anterior portion of the I3 muscle, or the "lip" of the slug, pinches down on the seaweed during the grasper protraction-open phase to reduce seaweed loss [15]. Our conclusions drawn about the different regions would change if the model incorporated some seaweed loss while the grasper is open. For example, the amount of seaweed ingested in regions **I-II** would be reduced, while the net seaweed movement in weak intake region **III** might approach zero.

The Shaw/Lyttle model was created as a biting and swallowing model. By controlling the timing of grasper closing, we were able to generate other behaviors such as rejection. In the model, the sequence of neural pools firing do not change regardless of the grasper behavior; however, the timing of certain neurons distinguishes ingestion and rejection behaviors *in vivo*. In particular, the motor neurons B8a, B8b, and B10 fire at different times in ingestion versus rejection [17]. Motor neurons B8a and B8b induce the grasper to close and are two of the neurons considered in neural pools a_1 and a_2 . The different activities in these two neurons during ingestion versus egestion is facilitated by interneurons: B20, B4/5, and cerebral-buccal interneuron 3 [6]. Although motor neuron B10 was not listed as a neuron in one of the neural pools, it is responsible for closing the jaws and facilitating grasper retraction. In addition to the motor neurons and interneurons, the onset of the radula nerve activity after the buccal nerve 2 activation can also serve to distinguish ingestion apart from rejection [16].

Thus, in a more detailed model, the sequencing and timing of the neural pools comprising the central pattern generator would change, as well as the timing of opening and closing relative to the different neural pools.

5.3 Future Directions

In order to investigate how rhythmic movements can be simultaneously robust and adaptable, the Shaw/Lyttle model was made to be sensitive to sensory feedback and changes in load, which are perturbations in the brain and the periphery, respectively. Throughout this thesis, we utilized this model to investigate how modulating the grasper affects the rate of seaweed movement (S) by systematically changing the parameters governing grasper closing condition. We have only experimented with a subset of all the parameters (Table 2, Appendix A.1). One of the ways to explore the model would be to vary the strength of sensory feedback (ϵ). In Chapter 3, we saw that the neural fixed points within the grasper-closed space determined the grasper behavior. Depending on its magnitude, strong sensory feedback may cause the trajectory to escape the fixed points faster, thereby affecting S . Another set of parameters to explore could be the muscle activation time constant (τ_m) and the maximum muscle activation (u_{\max}) parameters. We had applied the effects of neuromodulation on the opening and closing of the grasper, and manipulating τ_m and u_{\max} would explore the effects of neuromodulation on the reaction speed and power, respectively, produced by the I2 and I3 muscles.

In this thesis, we identified eight different parameter regions with different rates of seaweed movements and qualitatively different grasper behaviors. However, we have yet to determine

the rate of seaweed movement explicitly, so future developments could include deriving the rate of change S depending on other parameters such as F_{sw} , θ , δ , or μ . Currently, we numerically estimate S , so deriving the procedure to analytically calculate how S varies depending on other parameters would accelerate the research process as well as reveal other possibilities for experimentation.

Lyttle et al. [13] had observed a range of endogenous excitation values that cause the model to exhibit qualities from both the heteroclinic and the limit cycle regimes (Fig. 11 of [13]). We suspect that the grasper in the parameter regions determined in this thesis may behave differently within this range of endogenous excitation. Similarly, we expect the grasper to behave differently when the model is in the limit cycle regime. As the endogenous excitation increases, the trajectory moves away from the fixed points [22]. Consequently, there will be fewer (δ, θ) parameterizations that will have the grasper-closed space capture the trajectory, so we expect the area of region **IV** to increase while the size of other regions decrease. Changing the different parameter regions by varying the strength of μ would correspond to an interesting experiment on how the strength of the endogenous excitation can alter the way neuromodulation affects grasper behavior.

A Appendix

A.1 Parameters and Variables

Table 1: Model state variables and initial values. This table is modified from Table 2 of [13]. In the Shaw et al. model, the initial values are: $a_0 = 1 - 10^{-9}$, $a_1 = 10^{-9}$, $a_2 = 10^{-9}$, $u_0 = 0$, $u_1 = 0$, $x_r = 0.5$, and $x_{sw} = 0$. All quantities are dimensionless.

Variables	Value	Description
a_0	0.9003	activity of protraction-open neural pool
a_1	0.0836	activity of protraction-closing neural pool
a_2	0	activity of retraction-closed neural pool
u_0	0.7476	activity of I2 muscle
u_1	0.2463	activity of I3 muscle
x_r	0.6500	grasper position (0 is retracted, 1 is protracted)
x_{sw}	-8.2732	seaweed position (negative is towards the animal)

Table 2: Model parameters. This table is modified from Table 1 of [13]. In the Shaw/Lyttle model, $\mu = 10^{-9}$, $\epsilon = 2 \times 10^{-3}$, and $F_{sw} = 0.01$. All quantities are dimensionless.

Parameter	Value	Description
γ	2.4	inhibition strength from the next neural pool
ϵ	10^{-4}	sensory feedback strength
κ	$\frac{3\sqrt{3}}{2}$	length-tension curve normalization constant
μ	10^{-6}	neural pool intrinsic excitation
τ_a	0.05	neural pool time constant
τ_m	2.45	muscle activation time constant
b_r	0.1	grasper damping constant
b_{sw}	0.3	seaweed damping constant
c_0	1.0	position of shortest length for I2
c_1	1.1	position of center of I3
F_{sw}	0.1	force on the seaweed resisting ingestion
k_0	-1	I2 muscle strength and direction
k_1	1	I3 muscle strength and direction
σ_0	-1	sign of proprioceptive input to a_0 neural pool
σ_1	1	sign of proprioceptive input to a_1 neural pool
σ_2	1	sign of proprioceptive input to a_2 neural pool
S_0	0.5	proprioceptive neutral position for protraction-open neural pool
S_1	0.5	proprioceptive neutral position for protraction-closed neural pool
S_2	0.25	proprioceptive neutral position for retraction-closed neural pool
u_{max}	1.0	maximum muscle activation
w_0	2	maximal effective length of I2
w_1	1.1	maximal effective length of I3

A.2 Code

A.2.1 lyttle_model.m

Original code by Dr. Yangyang Wang to implement the Shaw et al. [22] and Lyttle et al. [13] model.

A.2.2 lyttle_model_vary_grasper.m

Code written by Dr. Peter Thomas through modifying lyttle_model.m by Dr. Yangyang Wang to allow varying of the grasper closing conditions.

A.2.3 lyttle_model_vary_grasper_run.m

```
% Script to run Dr. Yangyang Wang's version of the Lyttle model for different
% thresohld geometries and plot net seaweed intake rate.
%
% PJT w/ help from YYW 2019-11-01
% Graphing and other modifications by Hsing-Duan Louh
%% Start Parallel Workers
[status,hostname]=system('echo $HOSTNAME');
poolobj = gcp('ncreate');
if max(size(poolobj))==0
    if strcmp(hostname,'phase.MATH.CWRU.Edu')
        parpool(6) % start a pool of six workers if not already running
    else
        parpool(4) % start a pool of four workers if not already running
    end
end
end
%% S_rate_in
force=0.1; % default = force=.01;
nthresh=75;
clist=linspace(-.5,1.5,nthresh); % list of thresholds
dc = 2/(nthresh-1);
nangle=60;
alist=linspace(0,2*pi,nangle); % list of angles
da = 2*pi/(nangle-1);
[c,angle]=meshgrid(clist,alist);
S_rate_in=nan(nangle,nthresh);
nanRegions=zeros(nangle,nthresh);

for i=1:nthresh
    parfor j=1:nangle
        if isnan(S_rate_in(j,i))==1
            disp([j,i,nangle,nthresh])
```

```

M=lyttle_model_vary_grasper;
M.tmax=40;
M.yinit(8)=force; % Force is the 8th "variable".
M.ocangle=alist(j);
M.octhresh=clist(i)/sqrt(2);
M.solve;
t=M.t;
S=M.yext(:,7);
% discard trace for t<=10
idx_start=find(t>10,1,'first');
t=t(idx_start:end);
S=S(idx_start:end);

% Find where dS is zero.
dS=diff(S);
% Find last point where dS/dt=0
% (this is the open->close transition).
idx_end_of_flat=2+find(...
    (dS(1:end-2)==0).*...
    (dS(2:end-1)==0).*...
    (abs(dS(3:end))>0));
if ~isempty(idx_end_of_flat) %not empty
    i1=idx_end_of_flat(1);
    i2=idx_end_of_flat(end);
    % Net time
    delta_t=t(i2)-t(i1);
    % Net seaweed movement (let positive be inwards)
    delta_S=S(i1)-S(i2);
    % Rate
    S_rate_in(j,i)=delta_S/delta_t;
else
    i1=0; i2=0; delta_t=t(end)-t(1);
    delta_S=0;
    S_rate_in(j,i)=delta_S/delta_t;
end
end
else
    continue
end
end
end
% This is the saving protocol.
% Saving once very column to either lmv2 or lmv3
if mod(i,2)==0
    save lmv2
    display(sprintf('Now Completed column %d saved to lmv2',i))
    sound(y, Fs);
elseif mod(i,2)==1
    save lmv3
    display(sprintf('Now Completed column %d saved to lmv3',i))
else
    display('Error');
end
end
end
%% Intake Rate
da = 2*pi/(nangle-1);
dc = 2/(nthresh-1);
figure(1)
pcolor(clist-dc/2,(alist-da/2)/pi,S_rate_in)
hold on;
p2=plot(clist(38),alist(8)/pi,'r*','MarkerSize',12,'LineWidth',1.3)

```

```

set(gca,'FontSize',20)
xlabel('Threshold (\delta)')
ylabel('Angle (\theta/\pi)')
colormap hot
colorbar
%% Fixed Point Regions
%Load a a completed file such as lmv3 to run this section
da = 2*pi/(nangle-1);
dc = 2/(nthresh-1);
figure(2)
pcolor(clist-dc/2,(alist-da/2)/pi,S_rate_in)
hold on;
th=linspace(0,2*pi,201);
rp1=plot(zeros(length(th),1),th,'c--','Linewidth',4);
rp2=plot(sqrt(2)*cos(th),th/pi,'g-','Linewidth',4);
rp3=plot(sqrt(2)*sin(th),th/pi,'b--','Linewidth',4);
xlabel('Threshold (\delta)')
ylabel('Angle (\theta/\pi)')
LG=legend([rp1,rp2,rp3],{'a_0 Region','a_1 Region','a_2 Region'});
colormap hot
colorbar
ax=gca;
ax.FontSize=20;
LG.FontSize=14;
%% Distribution of Intake Rates
%Load a a completed file such as lmv3 to run this section
figure(3)
hist(S_rate_in(:),100)
ylabel('Frequency');
xlabel('Rate of Seaweed Movement');
ax=gca;
ax.FontSize=20;
%% Plot Sampled Points from Each Parameter Region (j,i)
%Load a a completed file such as lmv3 to run this section
da = 2*pi/(nangle-1);
dc = 2/(nthresh-1);
%Defining Colors for some sampled regions
orange=[0.9100,0.4100,0.1700];
pink=[1,0.4,0.6];
brown=[0.2 0 0];
figure(4)
pcolor(clist-dc/2,(alist-da/2)/pi,S_rate_in)
hold on;

% Plot horizontal and vertical lines intersecting at the sampled point
% Region I: Orange=(22,38)
plot(clist,alist(22)/pi*ones(nthresh,1),'w--')
plot(clist(38)*ones(nangle,1),alist/pi,'w--')

% Region II: Red=(8,38)
plot(clist,alist(8)/pi*ones(nthresh,1),'w--')
plot(clist(38)*ones(nangle,1),alist/pi,'w--')

% Region III: Green=(22,10)
plot(clist,alist(22)/pi*ones(nthresh,1),'w--')
plot(clist(10)*ones(nangle,1),alist/pi,'w--')

% Region IV: Pink=(11,72)
plot(clist,alist(11)/pi*ones(nthresh,1),'w--')

```

```

plot(clist(72)*ones(nangle,1),alist/pi,'w--')

% Region V: Cyan=(8,10)
plot(clist,alist(8)/pi*ones(nthresh,1),'w--')
plot(clist(10)*ones(nangle,1),alist/pi,'w--')

% Region VI: Brown=(50,33)
plot(clist,alist(50)/pi*ones(nthresh,1),'w--')
plot(clist(33)*ones(nangle,1),alist/pi,'w--')

% Region VII: Blue=(40,10)
plot(clist,alist(40)/pi*ones(nthresh,1),'w--')
plot(clist(10)*ones(nangle,1),alist/pi,'w--')

% Region VIII: Yellow=(50,10)
plot(clist,alist(50)/pi*ones(nthresh,1),'w--')
plot(clist(10)*ones(nangle,1),alist/pi,'w--')

%Plot all points again
p1=plot(clist(38),alist(22)/pi,'Color',orange,'Marker','s',...
'MarkerSize',10,'MarkerFaceColor',orange)
p2=plot(clist(38),alist(8)/pi,'-rs','MarkerSize',10,'MarkerFaceColor','r')
p3=plot(clist(10),alist(22)/pi,'-gs','MarkerSize',10,'MarkerFaceColor','g')
p4=plot(clist(72),alist(11)/pi,'Color',brown,'Marker','s',...
'MarkerSize',10,'MarkerFaceColor',brown)
p5=plot(clist(10),alist(8)/pi,'-cs','MarkerSize',10,'MarkerFaceColor','c')
p6=plot(clist(33),alist(50)/pi,'Color',pink,'Marker','s',...
'MarkerSize',10,'MarkerFaceColor',pink)
p7=plot(clist(10),alist(40)/pi,'-bs','MarkerSize',10,'MarkerFaceColor','b')
p8=plot(clist(10),alist(50)/pi,'-ys','MarkerSize',10,'MarkerFaceColor','y')

xlabel('Threshold (\delta)')
ylabel('Angle (\theta/\pi)')
LG=legend([p1,p2,p3,p4,p5,p6,p7,p8],...
{'I','II','III','IV','V','VI','VII','VIII'})
colormap gray
colorbar
ax=gca;
ax.FontSize=20;
LG.FontSize=14;

```

A.2.4 lyttle_model_state_var_plots.m

```

%Created by Hsing-Duan Louh, March 2020
clear all, close all
%% Evaluating the Grasper Trajectory
j=8; %Angle input
i=10; %Threshold input
force=0.1; % Seaweed force strength input
nthresh=75; nangle=60;
clist=linspace(-.5,1.5,nthresh); % list of thresholds
alist=linspace(0,2*pi,nangle); % list of angles
M=lyttle_model_vary_grasper;
M.tmax=40;
M.yinit(8)=force;
M.ocangle=alist(j);

```

```

M.octhresh=clist(i)/sqrt(2);
M.solve;

%% Plotting the Trajectory
ax1=subplot(2,2,1)
hold on;
plot(M.t,M.yext(:,1));
plot(M.t,M.yext(:,2));
plot(M.t,M.yext(:,3));
title('Neural Pool Activation');
legend('a0', 'a1', 'a2');
xlabel('Time (s)');
hold off;

%Muscle activations vs. time
ax2=subplot(2,2,2)
hold on;
plot(M.t,M.yext(:,4));
plot(M.t,M.yext(:,5));
title('Muscle Activation');
legend('I2', 'I3');
xlabel('Time (s)');
hold off;

%Grasper position vs. time
ax3=subplot(2,2,3);
hold on;
gBold=boldClose(M.yext(:,2),M.yext(:,3),M.yext(:,6),alist(j),clist(i));
hold on;
plot(M.t,M.yext(:,6),'k');
plot(M.t,gBold,'color',[0 0.5 0],'LineWidth',3);
hold off;
title('Grasper Position');
legend('Open', 'Closed');
xlabel('Time (s)');

%Seaweed position vs. time
ax4=subplot(2,2,4)
hold on;
plot(M.t,M.yext(:,7));
title('Seaweed Position');
xlabel('Time (s)');
hold off;

fs=17; %All axes fontsize
xfs=15; %x-axis FontSize

ax1.FontSize=fs;
ax1.YAxis.TickValues=[0,0.2,0.4,0.6,0.8,1];
ax1.XAxis.TickValues=[0,5,10,15,20,25,30,35,40];
ax1.YAxis.TickLength=[0.03,0.03];
ax1.XAxis.TickLength=[0.03,0.03];
ax1.XAxis.FontSize=xfs;

ax2.FontSize=fs;
ax2.YAxis.TickValues=[0,0.2,0.4,0.6,0.8,1];
ax2.XAxis.TickValues=[0,5,10,15,20,25,30,35,40];
ylim(ax2,[0,1]);
ax2.YAxis.TickLength=[0.03,0.03];

```

```

ax2.XAxis.TickLength=[0.03,0.03];
ax2.XAxis.FontSize=xf;

ax3.FontSize=fs;
ax3.YAxis.TickValues=[0,0.2,0.4,0.6,0.8,1];
ax3.XAxis.TickValues=[0,5,10,15,20,25,30,35,40];
ax3.YAxis.TickLength=[0.03,0.03];
ax3.XAxis.TickLength=[0.03,0.03];
ax3.XAxis.FontSize=xf;

ax4.FontSize=fs;
ax4.XAxis.TickValues=[0,5,10,15,20,25,30,35,40];
ax4.YAxis.TickLength=[0.03,0.03];
ax4.XAxis.TickLength=[0.03,0.03];
ax4.XAxis.FontSize=xf;

%Bold Grasper Position when the Grasper is closed
function dxr = boldClose(a1,a2,xr,theta,threshold)
%Return nan for when the grasper (xr) is open
cloStrength=cos(theta).*a1+sin(theta).*a2;
nanIdx=find(cloStrength<threshold);
dxr=xr;
dxr(nanIdx)=nan;
end

```

A.2.5 Fsw_vs_IntakeRate.m

```

% Code created by Hsing-Duan Louh January 2020
% The first section measures the periodic seaweed behavior with
% varying seaweed force and save each file
% Make sure to run each of the eight (i,j) combinations
% in the saving protocol at the end of this section
% The second section generates the plot for a single parameterization
% This section requires you to load data from one
% specific parameterization
% The third section compiles data from all eight regions into
% Fsw_vs_IntakeRate_all_zones.mat, this file is necessary for the
% fourth section. Therefore must have data
% from all eight regions compiled
% (regions listed in the saving protocol of first section)
% The fourth section requires loading Fsw_vs_IntakeRate_all_zones.mat
% before evaluating the graph of all regions together
%% Fsw impact on S_rate
clear all, close all
nthresh=75;
clist=linspace(-.5,1.5,nthresh); % list of thresholds
nangle=60;
alist=linspace(0,2*pi,nangle); % list of angles
[c,angle]=meshgrid(clist,alist);
nfs=101;
delta_S = zeros(1,nfs);
delta_t = zeros(1,nfs);
seaweed_force = linspace(-0.1,0.15,nfs); %list of seaweed forces
j=9;
i=38;
parfor w=1:length(seaweed_force)

```

```

display(w)
M=lyttle_model_vary_grasper;
M.tmax=40;
M.yinit(8)=seaweed_force(w); % Force is the 8th "variable".
M.ocangle=alist(j);
M.octhresh=clist(i)/sqrt(2);
M.solve;
t=M.t;
S=M.yext(:,7);
% discard trace for t<=10
idx_start=find(t>10,1,'first');
t=t(idx_start:end);
S=S(idx_start:end);
plot(t,S)
% Find where dS is zero.
dS=diff(S);
%Find last point where dS/dt=0 (this is the open->close transition).
idx_end_of_flat=2+find(...
    (dS(1:end-2)==0).*...
    (dS(2:end-1)==0).*...
    (abs(dS(3:end))>0));
if ~isempty(idx_end_of_flat) %not empty
    i1=idx_end_of_flat(1);
    i2=idx_end_of_flat(end);
    % Limit Cycle Period/Num of Periods
    delta_t(w)=(t(i2)-t(i1))/(length(idx_end_of_flat)-1);
    % Seaweed Movement per Period/Num of Periods
    delta_S(w)=(S(i1)-S(i2))/(length(idx_end_of_flat)-1);
else
    %If the seaweed movement is not periodic,
    i1=0; i2=0;
    delta_S(w)=0;
    delta_t(w)=t(end)-t(1);
end
end

%Saving Protocol for Different Regions
if j==22 && i==38
    save('Fsw_vs_IntakeRate_zone1_orange.mat');
elseif j==8 && i==38
    save('Fsw_vs_IntakeRate_zone2_red.mat');
elseif j==22 && i==10
    save('Fsw_vs_IntakeRate_zone3_green.mat');
elseif j==11 && i==72
    save('Fsw_vs_IntakeRate_zone4_pink.mat');
elseif j==8 && i==10
    save('Fsw_vs_IntakeRate_zone5_cyan.mat');
elseif j==50 && i==33
    save('Fsw_vs_IntakeRate_zone6_brown.mat');
elseif j==40 && i==10
    save('Fsw_vs_IntakeRate_zone7_blue.mat');
elseif j==50 && i==10
    save('Fsw_vs_IntakeRate_zone8_yellow.mat');
else
    display('Please adjust if-statement for (i,j) not listed ');
end

%% Single Region Analysis
figure(1) %Fsw vs S rate

```

```

plot(seaweed_force,delta_S./delta_t,'o-')
xlabel('Seaweed Force')
ylabel('Intake Rate')
title(strcat('Theta =',{ ' },num2str(alist(j)),{ ' },'Threshold =',...
    { ' },num2str(clist(i))))

figure(2) % Change in Seaweed Position and Period for Different Forces
hold on
plot(delta_t,delta_S,'o-')
xlabel('Period Duration (s)')
ylabel('Change in Seaweed Position')
title('Change in Seaweed Position per Period')

for th=linspace(-pi/2,pi/2,200),...
line([0 10*cos(th)],[0 40*sin(th)],end,shg)
ax=gca;
axis(ax);
ax.FontSize = 12;
ax.TickDir = 'out';
minW=min([first_deltaT,last_deltaT,first_deltaS,last_deltaS]);
maxW=max([first_deltaT,last_deltaT,first_deltaS,last_deltaS]);
hold off

%% Multiple Regions Comparison
%Compiling the saved data from the 8 sampled regions into
%Fsw_vs_IntakeRate_all_zones.mat

load Fsw_vs_IntakeRate_zone1_orange
Odelta_S=delta_S;
Odelta_t=delta_t;

load Fsw_vs_IntakeRate_zone2_red
Rdelta_S=delta_S;
Rdelta_t=delta_t;

load Fsw_vs_IntakeRate_zone3_green
Gdelta_S=delta_S;
Gdelta_t=delta_t;;

load Fsw_vs_IntakeRate_zone4_pink
Pdelta_S=delta_S;
Pdelta_t=delta_t;

load Fsw_vs_IntakeRate_zone5_cyan
Cdelta_S=delta_S;
Cdelta_t=delta_t;

load Fsw_vs_IntakeRate_zone6_brown
Brdelta_S=delta_S;
Brdelta_t=delta_t;
load Fsw_vs_IntakeRate_zone7_blue
Bldelta_S=delta_S;
Bldelta_t=delta_t;

load Fsw_vs_IntakeRate_zone8_yellow
Ydelta_S=delta_S;
Ydelta_t=delta_t;

```

```

save('Fsw_vs_IntakeRate_all_zones.mat');
%% Analyzing Multiple Datasets
load Fsw_vs_IntakeRate_all_zones.mat
figure(1) %Fsw vs S rate
hold on
plot(seaweed_force,Odelta_S./Odelta_t,'o-')
plot(seaweed_force,Rdelta_S./Rdelta_t,'o-')
plot(seaweed_force,Gdelta_S./Gdelta_t,'o-')
plot(seaweed_force,Pdelta_S./Pdelta_t,'o-')
plot(seaweed_force,Brdelta_S./Brdelta_t,'o-')
plot(seaweed_force,Bldelta_S./Bldelta_t,'o-')
plot(seaweed_force,Ydelta_S./Ydelta_t,'o-')
xlabel('Seaweed Force')
ylabel('Rate of Seaweed Movement (S)')
LG=legend('I','II','III','IV and V','VI','VII','VIII')
ax=gca;
ax.FontSize = 20;
LG.FontSize=14;

hold off;

figure(2) % Change in Seaweed Position and Period for Different Forces
hold on
p1=plot(Odelta_t,Odelta_S,'o-','LineWidth',1.5);
p2=plot(Rdelta_t,Rdelta_S,'o-','LineWidth',1.5);
p3=plot(Gdelta_t,Gdelta_S,'o-','LineWidth',1.5);
p4=plot(Pdelta_t,Pdelta_S,'o-','LineWidth',1.5);
p6=plot(Brdelta_t,Brdelta_S,'o-','LineWidth',1);
p7=plot(Bldelta_t,Bldelta_S,'o-','LineWidth',1);
p8=plot(Ydelta_t,Ydelta_S,'o-','LineWidth',1);
for th=linspace(-pi/2,pi/2,200),...
line([0 10*cos(th)],[0 40*sin(th)]),end,shg
ax=gca;
ax.FontSize = 20;
LG.FontSize=16;
ax.TickDir = 'out';
title('Change in Seaweed Position and Period for Different Forces');
xlabel('Period Duration (s)')
ylabel('Change in Seaweed Position')
legend('I','II','III','IV and V','VI','VII','VIII')
hold off;

```

A.2.6 RegionGeometry.m

```

%% Find regions where fixed points are included
%%Finding the fixed points that are within the closed region
%%By Hsing-Duan Louh Febrary 2020
force=0.1;
nthresh=75;
clist=linspace(-.5,1.5,nthresh); % list of thresholds
nangle=60;
alist=linspace(0,2*pi,nangle); % list of angles
regionGeometry=zeros(length(alist),length(clist));
dc = 2/(nthresh-1);
da = 2*pi/(nangle-1);
for j=1:length(alist)

```

```

for i=1:length(clist)
    val=0;
    beta=cos(alist(j));
    gamma=sin(alist(j));
    delta=clist(i);
    %testing a0 fixed point
    if 0 >= delta/sqrt(2)
        val=val+2;
    end
    %testing a1 fixed point
    if beta >= delta/sqrt(2)
        val=val+4;
    end
    %testing a2 fixed point
    if gamma >= delta/sqrt(2)
        val=val+8;
    end
    regionGeometry(j,i)=val;
end
end
figure(5)
pcolor(clist-dc/2,(alist-da/2)/pi,regionGeometry)
colormap jet
colorbar
xlabel('\delta = Threshold')
ylabel('Angle/\pi')
title('Fixed Points Regions');

```

A.2.7 Rate_of_change_of_differences_dzdt.m

```

% Figure 21 of the Thesis
% Evaluate the rate of change of the differences between trajectories
% on either side of the bifurcation in Region II.
% First and second sections evaluate forces and saves them separately
% Third section calculates the Jacobian symbolically and consolidates
% both files into one: 'Grasper_FBCompare_1-2.mat'.
% Note this Jacobian is for when the grasper is closed.
% Fourth section plots dz/dt or the rate of change of the differences.
% File by Hsing-Duan Louh
%% Trajectory for force less than the bifurcation force
j=8; %Angle of Region II
i=38; %Threshold of Region II
force=0.1161;
region='II';
nthresh=75; nangle=60;
clist=linspace(-.5,1.5,nthresh);
alist=linspace(0,2*pi,nangle);
M=lyttle_model_vary_grasper;
M.tmax=15;
M.yinit(8)=force;
M.ocangle=alist(j);
M.octhresh=clist(i)/sqrt(2);
M.solve;
save('Grasper_FB_1.mat');
%% Trajectory for force greater than the bifurcation force
j=8; %Angle of Region II

```

```

i=38; %Threshold of Region II
force=0.1162;
region='II';
nthresh=75; nangle=60;
clist=linspace(-.5,1.5,nthresh);
alist=linspace(0,2*pi,nangle);
M=lyttle_model_vary_grasper;
M.tmax=15;
M.yinit(8)=force;
M.ocangle=alist(j);
M.octhresh=clist(i)/sqrt(2);
M.solve;
save('Grasper_FB_2.mat');
%% Calculate the Jacobian of the Model Equations
% Jacobian for when the grasper is closed.
% Results saved to GrasperFB1-2.mat
% Calculate z=y1-y2
load Grasper_FB_1.mat
y1=M.yext(:,1:7);
times1=M.t;
load Grasper_FB_2.mat
y2=M.yext(:,1:7);
times2=M.t;

time=unique([times1;times2]); %Unique time discretizations
y1i=interp1q(times1,y1,time); %Interpolated y1
y2i=interp1q(times2,y2,time); %Interpolated y2
z=y2i-y1i;

load Grasper_FB_1.mat
%Parameters
mu=1e-6; % original standard value is 1e-5
tau_a=0.05; % time constant for neural activity
tau_m=2.45; % time constant for muscle activation
gamma=2.4;
eps=1e-4; % epsilon in the MS
s1=.5; % this is S0 in the MS
s2=.5; % this is S1 in the MS
s3=.25; % this is S2 in the MS
sig1=-1; % this is sigma0 in the MS
sig2=1; % this is sigma1 in the MS
sig3=1; % this is sigma2 in the MS
kappa=2.598076211353316; % This is the factor by which mu is reduced
% when seaweed is "present in the buccal cavity" i.e. during swallowing.
umax=1; % peak muscle activation
br=0.4; % grasper damping constant
k0=-1;
k1=1;
c0=1;
c1=1.1;
w0=2;
w1=1.1;
Fsw=0.145; %Parameter of interest

%Symbolically solve for the Jacobian
syms a0 a1 a2 u0 u1 xr xsw
v = [a0,a1,a2,u0,u1,xr,xsw];
F = [1./tau_a.*(a0.*(1-a0-gamma.*a1)+mu)+eps.*(xr-s1).*sig1,...
1./tau_a.*(a1.*(1-a1-gamma.*a2)+mu)+eps.*(xr-s2).*sig2,...

```

```

1./tau_a.*(a2.*(1-a2-gamma.*a0)+mu)+eps.*(xr-s3).*sig3,...
1./tau_m.*((a0+a1).*umax-u0),...
1./tau_m.*(a2.*umax-u1),...
(k0.*(-1.*kappa.*(xr-c0)./w0).*((xr-c0)./w0)-...
1).*((xr-c0)./w0+1)).*u0+...
k1.*(-1.*kappa.*(xr-c1)./w1).*((xr-c1)./w1)-...
1).*((xr-c1)./w1+1)).*u1+...
Fsw)./br,...
(k0.*(-1.*kappa.*(xr-c0)./w0).*((xr-c0)./w0)-...
1).*((xr-c0)./w0+1)).*u0+...
k1.*(-1.*kappa.*(xr-c1)./w1).*((xr-c1)./w1)-...
1).*((xr-c1)./w1+1)).*u1+...
Fsw)./br];
J=jacobian(F,v);
A=[]; %Storing Jacobian values
dzdt=[];
for w=1:size(z,1)
    input=y1i(w,:);
    A(:, :, w)=double(subs(J,v,input)); %Calculating each Jacobian
    dzdt(:, :, w)=A(:, :, w)*z(w,:)+0.0001/br*[0,0,0,0,1,1]';
    Az(:, :, w)=A(:, :, w)*z(w,:)' ;
end
% Grasper is open (manually determined) from M.t(1:292)
% These values have to be recalculated in the next 4 lines
% Since z = 0 when the grasper is open using our initial conditinos.
nanIdx=[1:292];
for n=1:length(nanIdx)
    dzdt(:, :, n)=A(:, :, n)*z(n,:)' ;
    Az(:, :, n)=A(:, :, n)*z(n,:)' ;
end
save('Grasper_FBCompare_1-2.mat')
%% Plot dz/dt
load Grasper_FBCompare_1-2.mat
% Reshape Data
rAz=reshape(Az,size(Az,1),size(Az,3));
rdzdt=reshape(dzdt,size(dzdt,1),size(dzdt,3));
idx=1;
%Run as long as |z|<=0(Fsw2-Fsw1)
while norm(z(idx,1:6))<=0.001
    idx=idx+1;
end
% select the appropriate time interval
t=time(1:idx);
rdzdt=rdzdt(:,1:idx);
rAz=rAz(:,1:idx);

fs=15; %All axes fontsize
xfs=15; %x-axis FontSize
sts=17; %Subplot title size

ax1=subplot(3,2,1);
hold on;
plot(t,rdzdt(1,:), 'LineWidth',2)
hold off;
title('a0');

ax2=subplot(3,2,2);
hold on;

```

```

plot(t,rdzdt(2,:), 'LineWidth',2)
hold off;
title('a1');

ax3=subplot(3,2,3);
hold on;
plot(t,rdzdt(3,:), 'LineWidth',2)
hold off;
title('a2');

ax4=subplot(3,2,4);
hold on;
plot(t,rdzdt(4,:), 'LineWidth',3)
plot(t,rdzdt(5,:), 'LineWidth',1.7)
title('Muscle Activation');
legend('I2', 'I3')
hold off;

ax5=subplot(3,2,5);
hold on;
plot(t,rdzdt(6,:), 'LineWidth',2)
hold off;
title('Grasper Position');
xlabel('Time (s)');

ax6=subplot(3,2,6);
hold on;
plot(t,rdzdt(7,:), 'LineWidth',2)
hold off;
title('Seaweed Position');
xlabel('Time (s)');

ylim(ax1, [-1e-3, 1e-3])
ylim(ax2, [-1e-3, 1e-3])
ylim(ax3, [-1e-3, 1e-3])
ylim(ax4, [-1e-3, 1e-3])
ylim(ax5, [-1e-3, 1e-3])
ylim(ax6, [-1e-3, 1e-3])

ax1.FontSize=fs;
ax1.YAxis.TickLength=[0.03,0.03];
ax1.XAxis.TickLength=[0.03,0.03];
ax1.Title.FontSize=sts;
ax1.XAxis.FontSize=xf;

ax2.FontSize=fs;
ax2.YAxis.TickLength=[0.03,0.03];
ax2.XAxis.TickLength=[0.03,0.03];
ax2.Title.FontSize=sts;
ax2.XAxis.FontSize=xf;

ax3.FontSize=fs;
ax3.YAxis.TickLength=[0.03,0.03];
ax3.XAxis.TickLength=[0.03,0.03];
ax3.Title.FontSize=sts;
ax3.XAxis.FontSize=xf;

```

```

ax4.FontSize=fs;
ax4.XAxis.TickLength=[0.03,0.03];
ax4.Title.FontSize=sts;
ax4.XAxis.FontSize=xf;

ax5.FontSize=fs;
ax5.XAxis.TickLength=[0.03,0.03];
ax5.Title.FontSize=sts;
ax5.XAxis.FontSize=xf;

ax6.FontSize=fs;
ax6.XAxis.TickLength=[0.03,0.03];
ax6.Title.FontSize=sts;
ax6.XAxis.FontSize=xf;
save('Grasper_FBCompare_1-2.mat');

```

A.2.8 grasperForceCompare.m

```

%Modify j, i, and force to compare grasper behavior of different regions
%at some seaweed force
%Generates Figure 23 in the Thesis
%File by Hsing-Duan Louh 2020
clear all, close all
j=[22,8,22,8,22]; %Parameter region input
i=[38,38,10,10,10]; %Parameter region input
force=0.1162; % Seaweed force input
region=["I","II","III","V","III"];
color=[0.9100,0.4100,0.1700;1,0,0;0,0.5,0;0,1,1;0,0.5,0];
for w=1:length(region)
    nthresh=75; nangle=60;
    clist=linspace(-.5,1.5,nthresh); % list of thresholds
    alist=linspace(0,2*pi,nangle); % list of angles
    M=lyttle_model_vary_grasper;
    M.tmax=2;
    M.yinit(8)=force; % Force is the 8th "variable"
    M.oangle=alist(j(w));
    M.octhresh=clist(i(w))/sqrt(2);
    M.solve;
    gBold=boldClose(M.yext(:,2),M.yext(:,3),...
    M.yext(:,6),alist(j(w)),clist(i(w)));
    figure(1)
    hold on;
    plot(M.t,M.yext(:,6),'color',color(w,:));
    h(w)=plot(M.t,gBold,'color',color(w,:), 'LineWidth',3);
    indx=find(0.99<=M.yext(:,3),1,'first');
    ll(w)=plot(M.t(indx),gBold(indx),'*', 'color', 'magenta',...
    'LineWidth',1.5, 'MarkerSize',7);
    ylabel('Grasper Position');
    xlabel('Time (s)');
    label=strcat('Grasper Behavior at Force =', " ",num2str(force));
    title(label);
end
ylim([0.6,1.1]);
plot([M.t(1),M.t(end)],ones(1,2),'--b', 'LineWidth',1.5)
ax=gca;
ax.FontSize=20;

```

```
h(5)=11(1);  
legend(h,{region(1),region(2),region(3),region(4),'High a2 Activity'})
```

References

- [1] Nicholas T Carnevale and Michael L Hines. *The NEURON book*. Cambridge University Press, 2006.
- [2] G Bard Ermentrout and David H Terman. *Mathematical foundations of neuroscience*, volume 35. Springer Science & Business Media, 2010.
- [3] Ronald M Harris-Warrick. Neuromodulation and flexibility in central pattern generator networks. *Current opinion in neurobiology*, 21(5):685–692, 2011.
- [4] Alan L Hodgkin and Andrew F Huxley. A quantitative description of membrane current and its application to conduction and excitation in nerve. *The Journal of physiology*, 117(4):500–544, 1952.
- [5] Eugene M Izhikevich and Jeff Moehlis. Dynamical systems in neuroscience: the geometry of excitability and bursting. *SIAM review*, 50(2):397, 2008.
- [6] Jian Jing and Klaudiusz R Weiss. Neural mechanisms of motor program switching in *Aplysia*. *Journal of neuroscience*, 21(18):7349–7362, 2001.
- [7] Eric R Kandel. The molecular biology of memory storage: a dialogue between genes and synapses. *Science*, 294(5544):1030–1038, 2001.
- [8] Paul S Katz. Intrinsic and extrinsic neuromodulation of motor circuits. *Current opinion in neurobiology*, 5(6):799–808, 1995.
- [9] Catherine E Kehl, Joey Wu, Sisi Lu, David M Neustadter, Richard F Drushel, Rebekah K Smoldt, and Hillel J Chiel. Soft-surface grasping: radular opening in *Aplysia californica*. *Journal of experimental biology*, 222(16):jeb191254, 2019.

- [10] Arthur D Kuo. The relative roles of feedforward and feedback in the control of rhythmic movements. *Motor control*, 6(2):129–145, 2002.
- [11] Edwin S Levitan, Richard H Kramer, and Irwin B Levitan. Augmentation of bursting pacemaker activity by egg-laying hormone in *Aplysia* neuron R15 is mediated by a cyclic AMP-dependent increase in Ca^{2+} and K^{+} currents. *Proceedings of the national academy of sciences*, 84(17):6307–6311, 1987.
- [12] Hui Lu, Jeffrey M McManus, and Hillel J Chiel. Extracellularly identifying motor neurons for a muscle motor pool in *Aplysia californica*. *JoVE (Journal of visualized experiments)*, (73):e50189, 2013.
- [13] David N Lyttle, Jeffrey P Gill, Kendrick M Shaw, Peter J Thomas, and Hillel J Chiel. Robustness, flexibility, and sensitivity in a multifunctional motor control model. *Biological cybernetics*, 111(1):25–47, 2017.
- [14] Eve Marder and Ronald L Calabrese. Principles of rhythmic motor pattern generation. *Physiological reviews*, 76(3):687–717, 1996.
- [15] Jeffrey M McManus, Hui Lu, and Hillel J Chiel. An *in vitro* preparation for eliciting and recording feeding motor programs with physiological movements in *Aplysia californica*. *JoVE (Journal of visualized experiments)*, (70):e4320, 2012.
- [16] Douglas W Morton and Hillel J Chiel. *In vivo* buccal nerve activity that distinguishes ingestion from rejection can be used to predict behavioral transitions in *Aplysia*. *Journal of comparative physiology A*, 172(1):17–32, 1993.

- [17] Douglas W Morton and Hillel J Chiel. The timing of activity in motor neurons that produce radula movements distinguishes ingestion from rejection in *Aplysia*. *Journal of comparative physiology A*, 173(5):519–536, 1993.
- [18] David M Neustadter, Richard F Drushel, Patrick E Crago, Benjamin W Adams, and Hillel J Chiel. A kinematic model of swallowing in *Aplysia californica* based on radula/odontophore kinematics and *in vivo* magnetic resonance images. *Journal of experimental biology*, 205(20):3177–3206, 2002.
- [19] Valerie A Novakovic, Gregory P Sutton, David M Neustadter, Randall D Beer, and Hillel J Chiel. Mechanical reconfiguration mediates swallowing and rejection in *Aplysia californica*. *Journal of comparative physiology A*, 192(8):857, 2006.
- [20] Mikhail I Rabinovich, Ramón Huerta, Pablo Varona, and Valentin S Afraimovich. Generation and reshaping of sequences in neural systems. *Biological cybernetics*, 95(6):519, 2006.
- [21] Christof J Schwiening. A brief historical perspective: Hodgkin and Huxley. *The Journal of physiology*, 590(11):2571–2575, 2012.
- [22] Kendrick M Shaw, David N Lyttle, Jeffrey P Gill, Miranda J Cullins, Jeffrey M McManus, Hui Lu, Peter J Thomas, and Hillel J Chiel. The significance of dynamical architecture for adaptive responses to mechanical loads during rhythmic behavior. *Journal of computational neuroscience*, 38(1):25–51, 2015.
- [23] Gregory P Sutton, Jonathan B Macknin, Steven S Gartman, George P Sunny, Randall D Beer, Patrick E Crago, David M Neustadter, and Hillel J Chiel. Passive hinge forces in

- the feeding apparatus of *Aplysia* aid retraction during biting but not during swallowing. *Journal of comparative physiology A*, 190(6):501–514, 2004.
- [24] Gregory P Sutton, Elizabeth V Mangan, David M Neustadter, Randall D Beer, Patrick E Crago, and Hillel J Chiel. Neural control exploits changing mechanical advantage and context dependence to generate different feeding responses in *Aplysia*. *Biological cybernetics*, 91(5):333–345, 2004.
- [25] Yangyang Wang, Jeffrey P Gill, Hillel J Chiel, and Peter J Thomas. Shape versus timing: linear responses of a limit cycle with hard boundaries under instantaneous and static perturbation. *arXiv preprint arXiv:1906.04387*, 2019.
- [26] Darren J Wilkinson. *Stochastic modelling for systems biology*. CRC press, 2018.
- [27] Sung-Nien Yu, Patrick E Crago, and Hillel J Chiel. Biomechanical properties and a kinetic simulation model of the smooth muscle I2 in the buccal mass of *Aplysia*. *Biological cybernetics*, 81(5-6):505–513, 1999.
- [28] Felix E Zajac. Muscle and tendon: properties, models, scaling, and application to biomechanics and motor control. *Critical reviews in biomedical engineering*, 17(4):359–411, 1989.